FENOC
FirstEnergy Nuclear Operating Company

Withhold Enclosure A from Public Disclosure under 10 CFR 2.390

When separated from Enclosure A, the remainder of this submittal may be decontrolled

Beaver Valley Power Station
P.O. Box 4
Shippingport, PA 15077

Paul A. Harden
Site Vice President

724-682-5234
Fax: 724-643-8069

February 18, 2011
L-11-024

10 CFR 50.90

ATTN: Document Control Desk
U. S. Nuclear Regulatory Commission
Washington, DC 20555-0001

SUBJECT:
Beaver Valley Power Station, Unit No. 2
Docket No. 50-412, License No. NPF-73
Chapters 5 and 7 of Holtec Licensing Report, In Support of License Amendment Request for Unit 2 Spent Fuel Pool Rerack (TAC No. ME1079)

By letter dated October 18, 2010 (Accession No. ML102940454), a revised request to amend the Beaver Valley Power Station Unit No. 2 (BVPS-2) Technical Specifications was submitted to support installation of high density fuel storage racks in the BVPS-2 spent fuel pool. Nonproprietary (Accession No. ML102940458) and proprietary versions of Revision 6 of the Holtec International Licensing Report for the BVPS-2 rerack were enclosed with that request. The submittal letter noted that Chapters 5 and 7 of the Holtec Report were not included and would be provided in a future submittal.

A proprietary version of Chapters 5 and 7 from Revision 8 of the Holtec International Licensing Report is provided in Enclosure A (the other chapters in the report are unchanged from the information docketed in the submittal dated October 18, 2010, and are not included herein). An affidavit from Holtec International, the owner of the information in the Licensing Report that is sought to be withheld pursuant to 10 CFR 2.390, is provided in Enclosure B. Enclosure C provides a nonproprietary version of Chapters 5 and 7 of the Licensing Report. FENOC requests that the proprietary information provided in Enclosure A be withheld from public disclosure.

Also, Attachment 1 provides clarification of information that was included in Enclosure A of the submittal dated October 18, 2010, regarding fuel cask area design.

There are no regulatory commitments contained in this letter. If there are any questions or if additional information is required, please contact Mr. Thomas A. Lentz, Manager – Fleet Licensing, at 330-761-6071.

A001
NRR

I declare under penalty of perjury that the foregoing is true and correct. Executed on February 18, 2011.

Sincerely,

Paul A. Harden

Attachments:

1. Revision to Enclosure A, Section 3.7 of the License Amendment Request for the Beaver Valley Power Station, Unit No. 2 Spent Fuel Pool Rerack

Enclosures:

A. Chapters 5 and 7 of the Licensing Report for the BVPS-2 Rerack (Proprietary Version)

B. 10 CFR 2.390 Affidavit for Holtec International Licensing Report Chapters 5 and 7, Revision 8

C. Chapters 5 and 7 of the Licensing Report for the BVPS-2 Rerack (Nonproprietary Version)

cc: NRC Region I Administrator (without Proprietary Enclosure)
NRC Resident Inspector Office (without Proprietary Enclosure)
NRC Project Manager (without Proprietary Enclosure)
Director BRP/DEP (without Proprietary Enclosure)
Site Representative BRP/DEP (without Proprietary Enclosure)

ATTACHMENT 1
L-11-024

Revision to Enclosure A, Section 3.7 of the License Amendment Request for the Beaver Valley Power Station, Unit No. 2 Spent Fuel Pool Rerack

By letter dated October 18, 2010 (Accession No. ML102940454), revised versions of the original evaluations were submitted to support installation of high density fuel storage racks in the Beaver Valley Power Station, Unit No. 2 (BVPS-2) spent fuel pool. The following information clarifies statements regarding fuel cask area design previously made on Enclosure A, page 11, of the October 2010 letter. Revision bars identify the added information.

The supporting evaluation also considered dropping items into the fuel cask area or onto the cover that will be placed over the fuel cask area during the installation of the new racks. All of the items to be installed in or over the fuel cask area weigh much less than a spent fuel cask, for which the fuel cask area was designed. The fuel cask area design includes a wall and gate, which physically separate the fuel cask area from the adjacent fuel storage pool. This physical separation prevents adverse effects on stored spent fuel assemblies in the fuel storage pool due to a spent fuel cask drop or a drop of a lighter load such as the fuel cask area platform or the fuel cask area fuel rack. FENOC has approved a procedure that requires the gate in this wall to be closed during installation and removal of either the fuel cask area platform or the fuel cask area fuel rack. As such, the drop of any of these items onto the floor of the fuel cask area would be bounded by a spent fuel cask drop (such load drops would not adversely affect fuel assemblies stored in the fuel storage pool due to the designed separation). With respect to drops onto the fuel that will temporarily be stored in the fuel cask area, the fuel cask area cover is designed to withstand the load imposed by a rack striking it from above. Since the fuel cask area cover would not fail due to this event, there cannot be any impact on the fuel assemblies in the rack below it. The evaluation also produced acceptable results for dropping any of the three parts of the fuel cask area cover onto the fuel loaded into the rack in the fuel cask area.

Enclosure B to FENOC Letter L-11-024

10 CFR 2.390 Affidavit for Holtec International Licensing Report Chapters 5 and 7, Revision 8

(Four pages follow)

HOLTEC INTERNATIONAL

Holtec Center, 555 Lincoln Drive West, Marlton, NJ 08053
Telephone (856) 797-0900
Fax (856) 797-0909

AFFIDAVIT PURSUANT TO 10 CFR 2.390

I, Richard J. Trotta, state as follows:

(1) I am the Holtec International Project Manager for the Beaver Valley Unit 2 Fuel Storage Racks Project and have reviewed the information described in paragraph (2) which is sought to be withheld, and am authorized to apply for its withholding.

(2) The information sought to be withheld is information provided with Holtec letter 1702-15, specifically Revision 7 and Revision 8 of Holtec Licensing Report HI-2084175, which contains Holtec Proprietary information and is appropriately marked as such.

(3) In making this application for withholding of proprietary information of which it is the owner, Holtec International relies upon the exemption from disclosure set forth in the Freedom of Information Act ("FOIA"), 5 USC Sec. 552(b)(4) and the Trade Secrets Act, 18 USC Sec. 1905, and NRC regulations 10CFR Part 9.17(a)(4), 2.390(a)(4), and 2.390(b)(1) for "trade secrets and commercial or financial information obtained from a person and privileged or confidential" (Exemption 4). The material for which exemption from disclosure is here sought is all "confidential commercial information", and some portions also qualify under the narrower definition of "trade secret", within the meanings assigned to those terms for purposes of FOIA Exemption 4 in, respectively, Critical Mass Energy Project v. Nuclear Regulatory Commission, 975F2d871 (DC Cir. 1992), and Public Citizen Health Research Group v. FDA, 704F2d1280 (DC Cir. 1983).

(4) Some examples of categories of information which fit into the definition of proprietary information are:

a. Information that discloses a process, method, or apparatus, including supporting data and analyses, where prevention of its use by Holtec's competitors without license from Holtec International constitutes a competitive economic advantage over other companies;

b. Information which, if used by a competitor, would reduce his expenditure of resources or improve his competitive position in the design, manufacture, shipment, installation, assurance of quality, or licensing of a similar product.

HOLTEC INTERNATIONAL

Holtec Center, 555 Lincoln Drive West, Marlton, NJ 08053
Telephone (856) 797-0900
Fax (856) 797-0909

c. Information which reveals cost or price information, production, capacities, budget levels, or commercial strategies of Holtec International, its customers, or its suppliers;

d. Information which reveals aspects of past, present, or future Holtec International customer-funded development plans and programs of potential commercial value to Holtec International;

e. Information which discloses patentable subject matter for which it may be desirable to obtain patent protection.

The information sought to be withheld is considered to be proprietary for the reason set forth in paragraph 4.a and 4.b, above.

(5) The information sought to be withheld is being submitted to the NRC in confidence. The information (including that compiled from many sources) is of a sort customarily held in confidence by Holtec International, and is in fact so held. The information sought to be withheld has, to the best of my knowledge and belief, consistently been held in confidence by Holtec International. No public disclosure has been made, and it is not available in public sources. All disclosures to third parties, including any required transmittals to the NRC, have been made, or must be made, pursuant to regulatory provisions or proprietary agreements which provide for maintenance of the information in confidence. Its initial designation as proprietary information, and the subsequent steps taken to prevent its unauthorized disclosure, are as set forth in paragraphs (6) and (7) following.

(6) Initial approval of proprietary treatment of a document is made by the manager of the originating component, the person most likely to be acquainted with the value and sensitivity of the information in relation to industry knowledge. Access to such documents within Holtec International is limited on a "need to know" basis.

(7) The procedure for approval of external release of such a document typically requires review by the staff manager, project manager, principal scientist or other equivalent authority, by the manager of the cognizant marketing function (or his designee), and by the Legal Operation, for technical content, competitive effect, and determination of the accuracy of the proprietary

HOLTEC INTERNATIONAL

Holtec Center, 555 Lincoln Drive West, Marlton, NJ 08053
Telephone (856) 797-0900
Fax (856) 797-0909

designation. Disclosures outside Holtec International are limited to regulatory bodies, customers, and potential customers, and their agents, suppliers, and licensees, and others with a legitimate need for the information, and then only in accordance with appropriate regulatory provisions or proprietary agreements.

(8) The information classified as proprietary was developed and compiled by Holtec International at a significant cost to Holtec International. This information is classified as proprietary because it contains detailed descriptions of analytical approaches and methodologies not available elsewhere. This information would provide other parties, including competitors, with information from Holtec International's technical database and the results of evaluations performed by Holtec International. A substantial effort has been expended by Holtec International to develop this information. Release of this information would improve a competitor's position because it would enable Holtec's competitor to copy our technology and offer it for sale in competition with our company, causing us financial injury.

(9) Public disclosure of the information sought to be withheld is likely to cause substantial harm to Holtec International's competitive position and foreclose or reduce the availability of profit-making opportunities. The information is part of Holtec International's comprehensive spent fuel storage technology base, and its commercial value extends beyond the original development cost. The value of the technology base goes beyond the extensive physical database and analytical methodology, and includes development of the expertise to determine and apply the appropriate evaluation process.

The research, development, engineering, and analytical costs comprise a substantial investment of time and money by Holtec International.

The precise value of the expertise to devise an evaluation process and apply the correct analytical methodology is difficult to quantify, but it clearly is substantial.

Holtec International's competitive advantage will be lost if its competitors are able to use the results of the Holtec International experience to normalize or verify their own process or if they are able to claim an equivalent understanding by demonstrating that they can arrive at the same or similar conclusions.

HOLTEC INTERNATIONAL

Holtec Center, 555 Lincoln Drive West, Marlton, NJ 08053
Telephone (856) 797-0900
Fax (856) 797-0909

AFFIDAVIT PURSUANT TO 10 CFR 2.390

The value of this information to Holtec International would be lost if the information were disclosed to the public. Making such information available to competitors without their having been required to undertake a similar expenditure of resources would unfairly provide competitors with a windfall, and deprive Holtec International of the opportunity to exercise its competitive advantage to seek an adequate return on its large investment in developing these very valuable analytical tools.

STATE OF NEW JERSEY)
) ss:
COUNTY OF BURLINGTON)

Mr. Richard J. Trotta, being duly sword, deposes and says:

That he has read the foregoing affidavit and the matters stated therein are true and correct to the best of his knowledge, information, and belief.

Executed at Marlton, New Jersey, this 11th day of February, 2011.

Richard J. Trotta
Holtec International

Subscribed and sword before me this 11 day of February, 2011.

JOANN TESCHKO
Commission # 2401629
Notary Public, State of New Jersey
My Commission Expires
October 22, 2015

Enclosure C to FENOC Letter L-11-024

Chapters 5 and 7 of the Licensing Report for the BVPS-2 Rerack (Nonproprietary Version)

(104 pages follow)

SUMMARY OF REVISIONS

Revision 0 – Original Revision.

Revision 1 – Incorporated Client comments in Chapters 4 and 6.

Revision 2 – Incorporated additional client comments throughout.

Revision 3 – Incorporated additional client comments in Chapters 1, 4, 5, 6, 8 and 9.

Revision 4 – Revised Chapter 4 including tables and figures based on revisions to analyses.

Revision 5 – Updated Chapters 2, 4, 5, 6, and 7 based on RAI responses and Client comments

Revision 6 – Chapters 5 and 7 have been removed. They may be added back into this report in next revision.

Revision 7 – Chapters 5 and 7 have been updated based on Supplemental RAI responses and Client comments and added to the report. The revision bars in Chapter 5 and 7 denote changes to the chapter relative to Revision 5.

Revision 8 – Minor editorial changes have been made to Chapters 5 and 7 to address client comments. The revision bars in the right hand margin of the document indicate the changes made in Revision 7 and Revision 8 (i.e., the revision bars from Revision 7 have not been deleted).

TABLE OF CONTENTS

TABLE OF CONTENTS (continued)

TABLE OF CONTENTS (continued)

LIST OF TABLES

LIST OF TABLES (continued)

LIST OF TABLES (continued)

LIST OF FIGURES

LIST OF FIGURES (continued)

LIST OF FIGURES (continued)

5.0 STRUCTURAL/SEISMIC CONSIDERATIONS

5.1 Introduction

This report provides information on the new spent fuel storage racks to support the license amendment process for the Beaver Valley Power Station (BVPS) Unit No. 2. This chapter, specifically, provides information on the required structural performance characteristics of the fuel storage racks.

5.2 Acceptance Criteria

To confirm the structural integrity of the racks, it is necessary to demonstrate compliance with the USNRC Standard Review Plan [5.1] and the OT Position Paper [5.2]. The rack structures are designed to meet the requirements of the ASME Code, Section III, Subsection NF for Class 3 linear-type supports. The relevant design criteria are discussed below, with additional details provided in the text associated with each analysis.

There are three principal design criteria, which must be satisfied by the rack modules:

a. Kinematic Criteria

According to Section 3.8.5 of Ref [5.1] and Ref [5.2], the minimum required safety margin against overturning under a Safe Shutdown Earthquake (SSE) event is 1.1. The margin of safety is defined here as the ratio of the rotation required to produce incipient tipping in either principal plane to the actual maximum rotation in that plane from the time history solution. The maximum rotations of the rack (about the two principal axes) are obtained from a post processing of the rack time history response output. All ratios from the SSE event should be greater than 1.1, to satisfy the regulatory acceptance criteria.

b. Stress Limit Criteria

The stress limits defined in ASME Code, Section III, Subsection NF must not be exceeded under the postulated load combinations. Load combinations are discussed in Section 5.3.

c. Fatigue Criteria

The cumulative damage factor, U, as defined in Section 5.6.9, must be shown to be less than or equal to 1.0.

5.3 Loads and Load Combinations

The applicable loads and their combinations that must be considered in the seismic analysis of rack modules are excerpted from Section 3.8.4 of Ref [5.1] and from Ref [5.2]. The load combinations considered are identified below along with their acceptance limits.

Load Combination	Acceptance Limit
$D + L$ $D + L + T_o$ $D + L + T_o + E$ (note 1)	Level A service limits
$D + L + T_a + E$ (note 1) $D + L + T_o + P_f$	Level B service limits
$D + L + T_a + E'$ (note 1)	Level D service limits
$D + L + F_d$	The functional capability of the racks should be demonstrated

Notes:

1) In addition to the acceptance limit given in the table above, the stresses induced in the rack modules due to this load combination must also be below the lesser of 2Sy or Su per Ref. [5.2] (where Sy is yield stress and Su is ultimate tensile stress).

Abbreviations are those used in Ref [5.1]:

D	=	Dead weight induced loads (including fuel assembly weight)
L	=	Live load (not applicable for the fuel rack, since there are no moving objects in the rack load path). Note that it is accepted practice to consider the fuel weight as a dead weight.
E	=	Operating Basis Earthquake (OBE)
E'	=	Safe Shutdown Earthquake (SSE)
T_o	=	Differential temperature induced loads, based on the most critical transient or steady state condition under normal operation or shutdown conditions.
T_a	=	Differential temperature induced loads, based on the postulated abnormal design conditions.
F_d	=	Force caused by the accidental drop of the heaviest load from maximum possible height. This load is considered to be an accident condition. The evaluation of this load condition is discussed in Chapter 7.
P_f	=	Force on the racks caused by postulated stuck fuel assembly. This load is considered to be an accident condition. The evaluation of this load condition is discussed in Chapter 7.

The differential temperature induced loads namely T_a and T_o, defined above, produce local thermal stresses. The worst thermal stress field in a fuel rack is obtained when an isolated storage location has a fuel assembly generating heat at maximum postulated rate and surrounding storage locations contain no fuel. Heated water makes unobstructed contact with the inside of the storage walls, thereby producing maximum possible temperature difference between adjacent cells. Secondary stresses produced are limited to the body of the rack; that is, support pedestals do not experience secondary (thermal) stresses. Thermal stresses are considered in Subsection 5.6.10.2 and conservatively combined with the primary stresses due to seismic loading to demonstrate compliance with Ref. [5.2].

5.4 Analysis Methods

In this section we describe the analysis methods to be used in performing calculations to demonstrate that the structural performance requirements for the fuel storage racks are satisfied. Similar structural analyses have been used for previous fuel storage rack licensing at many nuclear plants worldwide (see Table 5.4.1 for a partial list).

5.4.1 Overview of Rack Structural Analysis Methodology

The response of a freestanding rack module to seismic inputs is highly nonlinear and involves a complex combination of motions (sliding, rocking, twisting, and turning), resulting in impacts and friction effects. Some of the unique attributes of the rack dynamic behavior include a large fraction of the total structural mass in a confined rattling motion, friction support of rack pedestals against lateral motion, and large fluid coupling effects due to deep submergence and independent motion of closely spaced adjacent structures.

Linear methods, such as modal analysis and response spectrum techniques, cannot accurately simulate the structural response of such a highly nonlinear structure to seismic excitation. An accurate simulation is obtained only by direct integration of the nonlinear equations of motion with the three pool slab acceleration time-histories applied as the forcing functions acting simultaneously.

Whole Pool Multi-Rack (WPMR) analysis is the vehicle required to simulate the dynamic behavior of the complex spent fuel storage rack configuration.

The following sections provide the basis for this section and discussion on the development of the methodology.

5.4.1.1 Background of Analysis Methodology

Reliable assessment of the stress field and kinematic behavior of the rack modules calls for a conservative dynamic model incorporating all *key attributes* of the actual structure. This means that the model must feature the ability to execute the concurrent motion forms compatible with the freestanding installation of the modules.

The model must possess the capability to affect momentum transfers which occur due to rattling of fuel assemblies inside storage cells and the capability to simulate lift-off and subsequent impact of support pedestals with the underlying bearing pads. The contribution of the water mass in the interstitial spaces around the rack modules and within the storage cells must be modeled in an accurate manner, since erring in quantification of fluid coupling on either side of the actual value is no guarantee of conservatism.

The Coulomb friction coefficient at the pedestal-to-bearing pad interface may lie in a rather wide range and a conservative value of friction cannot be prescribed *a priori*. In fact, a perusal of results of rack dynamic analyses in numerous dockets (Table 5.4.1) indicates that an upper bound value of the coefficient of friction often maximizes the computed rack displacements as well as the equivalent elastostatic stresses.

In short, there are a large number of parameters with potential influence on the rack kinematics. The comprehensive structural evaluation must deal with all of these without sacrificing conservatism.

The three-dimensional single rack dynamic model introduced by Holtec International in the Enrico Fermi Unit 2 rack project (ca. 1980) and used in some 50 rerack projects since that time (Table 5.4.1) addresses most of the above-mentioned array of parameters. The details of this methodology are also published in the permanent literature [5.3]. Despite the versatility of the three dimensional seismic model, the accuracy of the single rack simulations has been suspect due to one key element; namely, hydrodynamic participation of water around the racks (not

applicable to the dry new fuel storage racks). During dynamic rack motion, hydraulic energy is either drawn from or added to the moving rack, modifying its submerged motion in a significant manner. Therefore, the dynamics of one rack affects the motion of all others in the pool.

A dynamic simulation, which treats only one rack, or a small grouping of racks, is intrinsically inadequate to predict the motion of rack modules submerged in water with any quantifiable level of accuracy. Three-dimensional Whole Pool Multi-Rack analyses carried out for many previous plants demonstrate that single rack simulations under predict rack displacement during seismic responses in a water environment [5.4].

Briefly, the 3-D rack model dynamic simulation, involving one or more spent fuel racks, handles the array of variables as follows:

Interface Coefficient of Friction: Parametric runs are made with upper bound and lower bound values of the coefficient of friction. The limiting values are based on experimental data, which have been found to be bounded by the values 0.2 and 0.8. Simulations are also performed with the array of pedestals having randomly chosen coefficients of friction in a Gaussian distribution with a mean of 0.5 and lower and upper limits of 0.2 and 0.8, respectively. In the fuel rack simulations, the Coulomb friction interface between rack support pedestal and bearing pad is simulated by piecewise linear (friction) elements. These elements function only when the pedestal is physically in contact with the bearing pad.

Rack Beam Behavior: Rack elasticity, relative to the rack base, is included in the model by introducing linear springs to represent the elastic bending action, twisting, and extensions.

Impact Phenomena: Compression-only gap elements are used to provide for opening and closing of interfaces such as the pedestal-to-bearing pad interface, and the fuel assembly-to-cell wall interface. These interface gaps are modeled using nonlinear spring elements. The term "nonlinear spring" is a generic term used to denote the mathematical representation of the condition where a restoring force is not linearly proportional to displacement.

Fluid Coupling: Holtec International extended Fritz's classical two-body fluid coupling model to multiple bodies and utilized it to perform the first two-dimensional multi-rack analysis (Diablo Canyon, ca. 1987). Subsequently, laboratory experiments were conducted to validate the multi-rack fluid coupling theory. This technology was incorporated in the Holtec-proprietary computer program DYNARACK [5.6], which handles simultaneous simulation of all racks in the pool as a Whole Pool Multi-Rack 3-D analysis. This development was first utilized in Chin Shan, Oyster Creek, and Shearon Harris plants [5.3, 5.5] and, subsequently, in numerous other rack projects. The WPMR analyses have corroborated the accuracy of the single rack 3-D solutions in predicting the maximum structural stresses, and also serve to improve predictions of rack kinematics.

For closely spaced racks, demonstration of kinematic compliance is verified by including all modules in one comprehensive simulation using a WPMR model. In WPMR analysis, all rack modules are modeled simultaneously and the coupling effect due to this multi-body motion is included in the analysis. Due to the superiority of this technique in predicting the dynamic behavior of closely spaced submerged storage racks, the Whole Pool Multi-Rack analysis methodology is used to analyze the spent fuel storage rack configurations.

5.4.2 WPMR Methodology

Recognizing that the analysis work effort must deal both with stress and displacement criteria, the sequence of model development and analysis steps that must be undertaken are summarized in the following:

a. Prepare 3-D dynamic models suitable for a time-history analysis of the fuel storage racks. These models include the assemblage of all rack modules in the spent fuel pool. Include all fluid coupling interactions and mechanical coupling appropriate to performing an accurate non-linear simulation. This 3-D simulation is referred to as a Whole Pool Multi-Rack model.

b. Perform 3-D dynamic analyses on various physical conditions (such as coefficient of friction and extent of cells containing fuel assemblies). Archive appropriate displacement and load outputs from the dynamic model for post-processing.

c. Perform stress analysis of high stress areas for the limiting case of all the rack dynamic analyses. Demonstrate compliance with ASME Code Section III, Subsection NF limits on stress and displacement.

5.4.2.1 Model Details for Racks

The dynamic modeling of the rack structure must be prepared with special consideration of all nonlinearities and parametric variations. Particulars of modeling details and assumptions for the WPMR analysis of racks are given in the following:

a. The fuel rack structure motion is captured by modeling the rack as a 12 degree-of-freedom structure. Movement of the rack cross-section at any height is described by six degrees-of-freedom of the rack base and six degrees-of-freedom at the rack top. In this manner, the response of the module, relative to the baseplate, is captured in the dynamic analyses once suitable springs are introduced to couple the rack degrees-of-freedom and simulate rack stiffness.

b. Rattling fuel assemblies within the rack are modeled by five lumped masses located at H, 0.75H, 0.5H, 0.25H, and at the rack base (H is the rack height measured above the baseplate). Each lumped fuel mass has two horizontal degrees-of-freedom. Vertical motion of the fuel assembly mass is assumed equal to rack vertical motion at the baseplate level. The centroid of each fuel assembly mass can be located off-center, relative to the rack structure centroid at that level, to simulate a partially loaded rack.

c. Seismic motion of a fuel rack is characterized by random rattling of fuel assemblies in their individual storage locations. The out of phase motion of the individual fuel assemblies has been appropriately considered by modifying the mass of the individual lumped masses discussed above.

d. Fluid coupling between the rack and fuel assemblies, and between the rack and wall, is simulated by appropriate inertial coupling in the system kinetic energy. Inclusion of these effects uses the methods of [5.9, 5.10] for rack-to-fuel coupling and for rack-to-rack coupling.

e. Fluid damping and form drag are conservatively neglected.

g. Potential impacts between the cell walls of the racks and the contained fuel assemblies are accounted for by appropriate compression-only gap elements between masses involved. The possible incidence of rack-to-wall or rack-to-rack impact is simulated by gap elements at the top and bottom of the rack in two horizontal directions. Bottom gap elements are located at the baseplate elevation.

The initial gaps reflect the presence of baseplate extensions, and the rack stiffnesses are chosen to simulate local structural detail.

h. The model for the rack is considered supported, at the base level, on four or five pedestals. Pedestals are modeled by non-linear compression gap elements in the vertical direction and as "rigid links" for transferring horizontal stress. Each pedestal support is linked to the bearing pad by two piecewise linear friction spring elements. These elements are properly located with respect to the centerline of the rack beam, and allow for arbitrary rocking and sliding motions. The spring rate for the friction springs includes any lateral elasticity of the stub pedestals. Local pedestal vertical spring stiffness accounts for floor elasticity and for local rack elasticity just above the pedestal.

i. Rattling of fuel assemblies inside the storage locations causes the gap between fuel assemblies and cell wall to change from a maximum of twice the nominal gap to a theoretical zero gap. Fluid coupling coefficients are based on the nominal gap in order to provide a conservative measure of fluid resistance to gap closure.

5.4.2.2 Element Details

Figure 5.1 shows a schematic of the dynamic model of a single rack. The schematic depicts many of the characteristics of the model including all of the degrees-of-freedom and most of the spring restraint elements.

Table 5.4.2 provides a complete listing of each of the 22 degrees-of-freedom for a rack model. Six translational and six rotational degrees-of-freedom (three of each type at top and bottom of rack) describe the motion of the rack structure. Rattling fuel mass motions (shown at nodes 1^*, 2^*, 3^*, 4^*, and 5^* in Figure 5.1) are described by ten horizontal translational degrees-of-freedom (two at each of the five fuel masses). The vertical fuel mass motion is assumed (and modeled) to be the same as that of the rack baseplate.

Figure 5.2 depicts the fuel to rack impact springs (used to develop potential impact loads between the fuel assembly mass and rack cell inner walls) in a schematic isometric. Only one of the five fuel masses is shown in this figure. Four compression-only springs, acting in the horizontal direction, are provided at each fuel mass.

Figure 5.3 provides a 2-D schematic elevation of the storage rack model, discussed in more detail in Section 5.4.2.4. This view shows the vertical location of the five storage masses and some of the support pedestal spring members.

Figure 5.4 shows the modeling technique and degrees-of-freedom associated with rack elasticity. In each bending plane a shear and bending spring simulate elastic effects [5.11]. Linear elastic springs coupling rack vertical and torsional degrees-of-freedom are also included in the model.

Figure 5.5 depicts the inter-rack impact springs (used to develop potential impact loads between racks or between rack and wall).

5.4.2.3 Multi-Body Fluid Coupling Phenomena

During the seismic event, all racks in the pool are subject to the input excitation in three orthogonal directions simultaneously. The motion of each freestanding module would be autonomous and independent of others as long as they did not impact each other and no water were present in the pool. While the scenario of inter-rack impact depends on rack spacing, the effect of water (the so-called fluid coupling effect) is a universal factor. As noted in Refs [5.10, 5.12], the fluid forces can reach rather large values in closely spaced rack geometries. It is, therefore, essential that the contribution of the fluid forces be included in a comprehensive manner for the spent fuel pool analyses. This is possible only if all racks in the pool are *allowed* to execute 3-D motion in the mathematical model. For this reason, single rack or even multi-rack models involving only a portion of the racks in the pool, are inherently inaccurate. The Whole Pool Multi-Rack model removes this intrinsic limitation of the rack dynamic models by simulating the 3-D motion of all modules simultaneously. The fluid coupling effect, therefore, encompasses interaction between *every* set of racks in the pool (i.e., the motion of one rack produces fluid forces on all other racks and on the pool walls). Stated more formally, both near-field and far-field fluid coupling effects are included in the analysis.

The derivation of the fluid coupling matrix [5.12] relies on the classical inviscid fluid mechanics principles, namely the principle of continuity and Kelvin's recirculation theorem. While the derivation of the fluid coupling matrix is based on no artificial construct, it has been nevertheless verified by an extensive set of shake table experiments [5.12].

In its simplest form, the so-called "fluid coupling effect" [5.9, 5.10] can be explained by considering the proximate motion of two bodies under water. If one body (mass m_1) vibrates adjacent to a second body (mass m_2), and both bodies are submerged in frictionless fluid, then Newton's equations of motion for the two bodies are:

$$(m_1 + M_{11})\, A_1 + M_{12}\, A_2 = \text{applied forces on mass } m_1 + O(X_1^2)$$
$$M_{21}\, A_1 + (m_2 + M_{22}) A_2 = \text{applied forces on mass } m_2 + O(X_2^2)$$

A_1, A_2 denote absolute accelerations of masses m_1 and m_2, respectively, and the notation $O(X^2)$ denotes nonlinear terms.

M_{11}, M_{12}, M_{21}, and M_{22} are fluid coupling coefficients which depend on body shape, relative disposition, etc. Fritz [5.10] gives data for M_{ij} for various body shapes and arrangements. The fluid adds mass to the body (M_{11} to mass m_1), and an inertial force proportional to acceleration of the adjacent body (mass m_2). Thus, acceleration of one body affects the force field on another. This force field is a function of inter-body gap, reaching large values for small gaps. Lateral motion of a fuel assembly inside a storage location encounters this effect. For example, fluid coupling behavior will be experienced between nodes 2 and 2* in Figure 5.1. The rack analysis also contains inertial fluid coupling terms, which model the effect of fluid in the gaps between adjacent racks.

Rack-to-rack gap elements have initial gaps set to 100% of the physical gap between the racks or between outermost racks and the adjacent pool walls.

5.4.2.4 Stiffness Element Details

Three element types are used in the rack models. Type 1 elements represent the linear elastic beam-like behavior of the integrated rack cell matrix. Type 2 elements are the piecewise linear friction springs used to develop the appropriate horizontal forces between the rack pedestals and the supporting bearing pads. Type 3 elements are non-linear gap elements, which model gap closures and subsequent impact loadings (i.e., between fuel assemblies and the storage cell inner walls, rack outer periphery spaces and the vertical forces between the rack pedestals and the supporting bearing pads).

If the simulation model is restricted to two dimensions (one horizontal motion plus one vertical motion, for example), for the purposes of model clarification only, then Figure 5.3 describes the configuration. This simpler model is used to elaborate on the various stiffness modeling elements.

Type 3 gap elements modeling impacts between fuel assemblies and racks have local stiffness K_i in Figure 5.3. Support pedestal spring rates K_S are modeled by type 3 gap elements. Local compliance of the concrete floor is included in K_S. The type 2 friction elements are shown in Figure 5.3 as K_f. The spring elements depicted in Figure 5.4 represent type 1 elements.

Friction at the support/bearing pad interface is modeled by the piecewise linear friction springs with suitably large stiffness K_f up to the limiting lateral load μN, where N is the current compression load at the interface between support and bearing pad. At every time-step during transient analysis, the current value of N (either zero if the pedestal has lifted off the bearing pad, or a compressive finite value) is computed.

The gap element K_S, modeling the effective compression stiffness of the structure in the vicinity of the support, includes stiffness of the pedestal, local stiffness of the underlying pool slab, and local stiffness of the rack cellular structure above the pedestal.

The previous discussion is limited to a 2-D model solely for simplicity. Actual analyses incorporate 3-D motions.

5.4.2.5 Coefficients of Friction

To eliminate the last significant element of uncertainty in rack dynamic analyses, multiple simulations must be performed to adjust the friction coefficient ascribed to the support pedestal/ bearing pad interface. These friction coefficients are chosen consistent with the two bounding extremes from Rabinowicz's data [5.8]. Simulations are also performed by imposing intermediate value friction coefficients developed by a random number generator with Gaussian normal distribution characteristics. The assigned values are then held constant during the entire simulation in order to obtain reproducible results.[†] Thus, in this manner, the WPMR analysis results are brought closer to the realistic structural conditions.

The coefficient of friction (μ) between the pedestal supports and the pool floor is indeterminate. According to Rabinowicz [5.8], results of 199 tests performed on austenitic stainless steel plates submerged in water show a mean value of μ to be 0.503 with standard deviation of 0.125. Upper and lower bounds (based on twice standard deviation) are 0.753 and 0.253, respectively. Analyses are therefore performed for coefficient of friction values of 0.2 (lower limit) and for 0.8 (upper limit), and for random friction values clustered about a mean of 0.5. The bounding values of $\mu = 0.2$ and 0.8 have been found to envelope the upper limit of module response in previous rerack projects.

[†] It is noted that DYNARACK has the capability to change the coefficient of friction at any pedestal at each instant of contact based on a random reading of the computer clock cycle. However, exercising this option would yield results that could not be reproduced. Therefore, the random choice of coefficients is made only once per run.

5.4.2.6 Governing Equations of Motion

Using the structural model discussed in the foregoing, equations of motion corresponding to each degree-of-freedom are obtained using Lagrange's Formulation [5.11]. The system kinetic energy includes contributions from solid structures and from trapped and surrounding fluid. The final system of equations obtained has the matrix form:

$$[M]\left[\frac{d^2 q}{d t^2}\right] = [Q] + [G]$$

where:

[M] is the total mass matrix (including structural and fluid mass contributions). The size of this matrix will be 22n x22n for a WPMR analysis (n = number of racks in the model).

q is the nodal displacement vector relative to the pool slab displacement (the term with q indicates the second derivative with respect to time, i.e., acceleration)

[G] is a vector dependent on the given ground acceleration

[Q] is a vector dependent on the spring forces (linear and nonlinear) and the coupling between degrees-of-freedom

The above column vectors have length 22n. The equations can be rewritten as follows:

$$\left[\frac{d^2 q}{d t^2}\right] = [M]^{-1}[Q] + [M]^{-1}[G]$$

This equation set is mass uncoupled, displacement coupled at each instant in time. The numerical solution uses a central difference scheme built into the Holtec-proprietary computer program DYNARACK [5.6].

5.5 Structural Evaluation of Racks

To provide a demonstration that the proposed rack layouts and rack designs (see Chapters 1 and 2) will appropriately satisfy the requirements discussed in the preceding sections of this chapter, a series of structural evaluations have been performed and are described in the remaining sections.

5.5.1 Description of Rack Layout

The various components for each of the rack styles are described in detail in Section 2.6. The models prepared for the DYNARACK simulations account for all of the pertinent features and characteristics of each rack. Rack material is defined in Table 5.4.3.

The cartesian coordinate system utilized within the dynamic models has the following orientation:

x = Horizontal axis along plant North (in a north-south direction)
y = Horizontal axis along plant East (in an east-west direction)
z = Vertical axis upward from the rack base

For the dynamic rack simulations, the dry fuel weight is conservatively taken to be 1,616 lbs to account for the maximum fuel weight at every location.

5.5.2 Synthetic Time-Histories

Synthetic time-histories in three orthogonal directions (N-S, E-W, and vertical) were generated in accordance with the provisions of Section 3.7.1 of the SRP [5.1]. In order to prepare an acceptable set of acceleration time-histories, the Holtec-proprietary code GENEQ [5.7] was utilized. As required by the recent issue of the SRP [5.1], the code GENEQ was used to develop five sets of acceleration time histories for the design basis response spectra.

The following criteria required by SRP Section 3.7.1 have been satisfied:

1. Each time history set (2 horizontal and 1 vertical) must be statistically independent. This is demonstrated by calculating the cross correlation coefficient for each time history with each of the other two events. The absolute value of each of the three correlation coefficients must be less than 0.16.

2. For each of the time histories:

   - The time history shall have a sufficiently small time increment and sufficiently long duration. Records shall have a Nyquist frequency of at least 50 Hz, (e.g., a time increment of at most 0.010 seconds) and a total duration of at least 20 seconds.

   - Spectral acceleration at 5% damping shall be computed at a minimum of 100 points per frequency decade, uniformly spaced over the log frequency scale from 0.1 Hz to 50 Hz or the Nyquist frequency. The comparison of the response spectrum obtained from the artificial ground motion time history with the target response spectrum shall be made at each frequency computed in the frequency range of interest.

3. For each of the *average* response spectra:

   - The computed 5% damped response spectrum of the accelerogram shall not fall more than 10% below the target response spectrum at any one frequency.

   - The computed 5% damped response spectrum of the artificial ground motion time history shall not exceed the target response spectrum at any frequency by more than 30% (a factor of 1.3) in the frequency range of interest. If the response spectrum for the accelerogram exceeds the target response spectrum by more than 30% at any frequency range, the power spectrum density of the accelerogram needs to be computed and shown to not have significant gaps in energy at any frequency over this frequency range.

5.5.3 Stress Limit Evaluations

The stress limits presented below apply to the rack structure and are derived from the ASME Code, Section III, Subsection NF [5.13]. Parameters and terminology are in accordance with the ASME Code. Upset loads (Level B) are conservatively evaluated against ASME Level A stress limits. Material properties are obtained from the ASME Code Section II, Part D [5.16], and are listed in Table 5.4.3.

(i) Normal and Upset Conditions (Level A or Level B)

a. Allowable stress in tension on a net section is:

$F_t = 0.6\ S_y$

where, S_y = yield stress at temperature, and F_t is equivalent to primary membrane stress.

b. Allowable stress in shear on a net section is:

$F_v = .4\ S_y$

c. Allowable stress in compression on a net section is:

$$F_a = S_y\left(.47 - \frac{k\,\ell}{444\,r}\right)$$

where kl/r for the main rack body is based on the full height and cross section of the honeycomb region and does not exceed 120 for all sections.

l = unsupported length of component

k = length coefficient which gives influence of boundary conditions. The following values are appropriate for the described end conditions:

1 (simple support both ends)

2 (cantilever beam)

½ (clamped at both ends)

r = radius of gyration of component

d. Maximum allowable bending stress at the outermost fiber of a net section, due to flexure about one plane of symmetry is:

$F_b = 0.60\ S_y$ (equivalent to primary bending)

e. Combined bending and compression on a net section satisfies:

$$\frac{f_a}{F_a} + \frac{C_{mx}\, f_{bx}}{D_x\, F_{bx}} + \frac{C_{my}\, f_{by}}{D_y\, F_{by}} < 1$$

where:

f_a = Direct compressive stress in the section

f_{bx} = Maximum bending stress along x-axis

f_{by} = Maximum bending stress along y-axis

C_{mx} = 0.85

C_{my} = 0.85

D_x = $1 - (f_a/F'_{ex})$

D_y = $1 - (f_a/F'_{ey})$

$F'_{ex,ey}$ = $(\pi^2\, E)/(2.15\ (kl/r)^2_{x,y})$

E = Young's Modulus

and subscripts x,y reflect the particular bending plane.

f. Combined flexure and compression (or tension) on a net section:

$$\frac{f_a}{0.6\, S_y} + \frac{f_{bx}}{F_{bx}} + \frac{f_{by}}{F_{by}} < 1.0$$

The above requirements are to be met for both direct tension or compression.

g. Welds

Allowable maximum shear stress on the net section of a weld is given by:

$F_w = 0.3\ S_u$

where S_u is the weld material ultimate strength at temperature. For fillet weld legs in contact with base metal, the shear stress on the gross section is limited to $0.4S_y$, where S_y is the base material yield strength at temperature.

(ii) Level D Service Limits

Section F-1334 (ASME Section III, Appendix F) [5.14], states that the limits for the Level D condition are the minimum of 2 or 1.167 S_u/S_y times the corresponding limits for the Level A condition if $S_u > 1.2S_y$, or 1.4 if $S_u \leq 1.2S_y$ except for requirements specifically listed below. S_u and S_y are the ultimate strength and yield strength at the specified rack design temperature. Examination of material properties for 304 and 304L stainless demonstrates that the $S_u > 1.2S_y$ condition above is met.

Exceptions to the above general multiplier are the following:

a) Stresses in shear shall not exceed the lesser of $0.72S_y$ or $0.42S_u$. In the case of the Austenitic Stainless material used here, $0.72S_y$ governs.

b) Axial Compression Loads shall be limited to 2/3 of the calculated buckling load.

c) Combined Axial Compression and Bending - The equations for Level A conditions shall apply except that:

F_a = 0.667 x Buckling Load/ Gross Section Area,

and the terms F'_{ex} and F'_{ey} may be increased by the factor 1.65.

d) For welds, the Level D allowable maximum weld stress is not specified in Appendix F of the ASME Code. An appropriate limit for weld throat stress is conservatively set here as:

$F_w = (0.3\ S_u)$ x factor

where:

factor = (Level D shear stress limit)/(Level A shear stress limit)

= 0.72 x Sy / 0.4 x Sy = 1.8

5.5.3.1 Dimensionless Stress Factors

For convenience, the stress results are presented in dimensionless form. Dimensionless stress factors are defined as the ratio of the actual developed stress to the specified limiting value. The limiting value of each stress factor is 1.0.

Stress factors reported are:

R_1	=	Ratio of direct tensile or compressive stress on a net section to its allowable value (note pedestals only resist compression)
R2	=	Ratio of gross shear on a net section in the x-direction to its allowable value
R3	=	Ratio of maximum x-axis bending stress to its allowable value for the section
R4	=	Ratio of maximum y-axis bending stress to its allowable value for the section
R5	=	Combined flexure and compressive factor (as defined in the foregoing)
R6	=	Combined flexure and tension (or compression) factor (as defined in the foregoing)
R7	=	Ratio of gross shear on a net section in the y-direction to its allowable value.

5.5.4 Parametric Simulations

Comprehensive 3-D acceleration-time history analyses were performed for the SSE and OBE design basis event. The following rack configurations (cases) have been analyzed for Spent Fuel Racks:

1) Whole Pool Multi Rack Configuration: This configuration is used for the spent fuel racks in the spent fuel pool. All the racks in the spent fuel pool are included in the seismic analysis with appropriate surrounding gaps.

2) Single Rack Configuration: In order to evaluate the structural integrity of the cask pit platform and assess the seismic amplification due to the dynamic characteristics of the cask pit platform, an additional dynamic analysis is performed using a coupled rack-platform model. The cask pit platform is a beam like structure which temporarily supports a single loaded rack during the SFR loading campaign. The analysis method, and the analysis code used to perform this analysis, is identical to the WPMR analysis method except that the model includes just a single rack (as opposed to all racks in the pool) and one additional body representing the cask pit platform. The cask pit platform is modeled as a six degree of freedom rectangular body of appropriate size and mass, which is capable of twisting, rocking, and sliding relative to the cask pit floor. In the coupled model, the spent fuel rack sits atop the platform in a freestanding manner. A combination of non-linear gap elements and friction elements are used to define the contact interfaces between the rack support pedestals and the platform, and the platform and the cask pit floor. Figure 5.6 shows a schematic of the coupled model, which is implemented using the computer program DYNARACK. Since a random COF is shown to bound the WPMR analysis, the random COF is used in the single rack analysis.

The following presents a complete listing of the simulations discussed herein. Consideration of the parameters described in Section 5.4.2 resulted in the following runs.

LIST OF SPENT FUEL RACK SIMULATIONS				
Run	Model	Load Case	COF	Event
1	WPMR	All Racks Fully Loaded	0.2	SSE, Set 4
2	WPMR	All Racks Fully Loaded	Random	SSE, Set 4
3	WPMR	All Racks Fully Loaded	0.8	SSE, Set 4
4	WPMR	All Racks Fully Loaded	0.2	OBE, Set 4
5	WPMR	All Racks Fully Loaded	Random	OBE, Set 4
6	WPMR	All Racks Fully Loaded	0.8	OBE, Set 4
7♦	Single Rack	Fully Loaded Rack	Random	SSE, Set 4
8	WPMR	Partially Loaded Racks	Random	SSE, Set 4

where Random = Gaussian distribution with a mean of 0.5 coefficient of friction and upper and lower limits of 0.8 and 0.2.

Figure 5.7 shows the partially loaded rack configuration that is analyzed in run number 8.

5.6 Mechanical Evaluation of Racks

This section discusses the results of the structural analysis of the racks and the mechanical evaluation performed to show that the acceptance criteria, discussed in Section 5.2, are met. The evaluation of the racks to address their ability to withstand the postulated mechanical accidents is discussed in Chapter 7.

♦ Since Set 4 seismic event (i.e. run 2) produces the largest stresses in the rack modules, the single rack analysis is run with Set 4 seismic event as well for conservatism.

The results from the DYNARACK runs are provided in this section by extracting the worst case values from the parameters of interest; namely displacements, support pedestal forces, impact loads, and stress factors. This section also summarizes other analyses performed to develop and evaluate structural member stresses, which are not determined by the DYNARACK postprocessor.

5.6.1 Rack Displacements

The largest top of rack displacement for the spent fuel rack configurations considered is 2.79". Other simulations have smaller, but comparable, displacements in both x and y directions.

By comparison of the maximum displacement with the minimum width of the rack, which is approx. 81" per Table 2.1.1, it is obvious that rack overturning is of no concern and the required safety factor against the overturning of 1.1 will be easily exceeded.

5.6.2 Pedestal Vertical Forces

The highest vertical pedestal load from all spent fuel racks is 326,000 lbs, which bounds all simulations.

5.6.3 Pedestal Friction Forces

The maximum friction load for the spent fuel racks in either x or y direction is 122,000 lbs. This load has been used to evaluate the female pedestal-to-baseplate weld, as discussed in Section 5.6.7 (part b).

5.6.4 Rack Impact Loads

A freestanding rack, by definition, is a structure subject to potential impacts during a seismic event. Impacts arise from rattling of the fuel assemblies in the storage rack locations and, in some instances, from localized impacts between the racks, or between a peripheral rack and the pool wall. The following sections discuss the bounding values of these impact loads.

5.6.4.1 Rack Impacts

In order to protect the rack cell structure from impact during a seismic event and maintain the proper rack spacing, the rack baseplates extend beyond the perimeter envelope of the cell region. The racks are then installed in the pool with a very small separation between adjacent rack baseplates. Therefore, by design the racks are predisposed to impact each other at the baseplate level during a seismic event, rather than at the top of rack elevation. As a result, the 3/4 inch thick rack baseplates have been designed to accommodate the in-plane contact forces.

The impact loads at the rack base are experienced on the perimeter edges of the baseplates and are insignificant compared to the plate capacity in compression. Local deformations will result in the impact load being spread across a substantial width of the entire baseplate. Rack to rack impacts do occur at the top of rack elevation between adjacent spent fuel racks at several locations in the spent fuel pool. The maximum rack to rack impact load at rack top is 101,800 lb observed between racks A2 and A3. A buckling failure analysis of the impacted racks has been performed using the computer code LS-DYNA, and the safety factor against buckling collapse of the storage cells has been determined to be greater than 1.5 for the maximum rack to rack impact load, which satisfies the axial compression limit under faulted conditions per F-1334.3 [5.14].

No rack-to-wall impacts occur in any of the dynamic simulations. Thus, the freestanding racks do not transmit any forces to the SFP walls.

5.6.4.2 Fuel to Cell Wall Impact Loads

Even though limits on secondary stresses are not prescribed in the ASME Code for Class 3 NF structures, evaluations must be made to ensure that the localized impacts do not lead to plastic deformations in the storage cells which affect the sub-criticality of the stored fuel array. Local cell wall integrity is conservatively estimated from peak impact loads. Plastic analysis is used to obtain the limiting impact load, which would lead to gross permanent deformation.

A review of all simulations performed allows determination of the maximum instantaneous impact load between fuel assembly and fuel cell wall at any modeled impact site. For the spent fuel racks with a wall thickness of 0.075", the limiting side load is 3,204 lbs. The maximum fuel assembly impact load is 610.2 lbs. Therefore, the cell walls are structurally adequate.

5.6.5 Rack Stress Factors

The time history results from the DYNARACK solver provide the pedestal normal and lateral interface forces, which may be converted to the limiting bending moment and shear force at the bottom baseplate-pedestal interface. In particular, maximum values for the previously defined stress factors are determined for every pedestal in the array of racks. The net section maximum (in time) bending moments and shear forces can also be determined at the bottom baseplate-rack cellular structure interface for each spent fuel rack in the pool. Using these forces and moments, the maximum stress in the limiting rack cell (box) can be evaluated.

The stress factor results for male and female pedestals, and for the entire spent fuel rack cellular cross section just above the baseplate have been determined. These factors are reported for every rack in each simulation, and for each pedestal in every rack. These locations are the most heavily loaded net sections in the structure so that satisfaction of the stress factor criteria at these locations ensures that the overall structural criteria set forth in Section 5.5.3 are met.

For the spent fuel racks, the maximum stress factor for the DYNARACK simulations is 0.888, which occurs in the cellular region of the rack and conservatively accounts for the effective width of the cell wall based on its slenderness ratio. This calculated value of stress factor is less than the allowable of 1.0. The maximum stress factor computed for the rack supports is less than computed for the cellular region and obviously less than the allowable of 1.0.

The stress factors, as defined in Subsection 5.5.3.1, for all of the simulations performed, leads to the conclusion that all stress factors are less than the mandated limit. Therefore, the requirements of Section 5.2 are satisfied for the load levels considered for every limiting location in the racks.

5.6.6 Pedestal Thread Shear Stress

For the Spent Fuel Racks the maximum average shear stress in the engagement region is 8,684 psi and 11,555 psi for OBE and SSE, respectively. These stresses are bounding for both the male and female pedestal threads. The allowable shear stress for Level A conditions is 0.4 Sy = 10,000 psi (based on Sy for SA240-304 at 200°F). The allowable shear stress for Level D conditions is the lesser of: 0.72 S_y = 18,000 psi or 0.42 S_u = 29,400 psi (based on S_y and S_u for SA240-304 at 200°F).

5.6.7 Weld Stresses

Weld locations subjected to significant seismic loading are located at the bottom of the rack at the baseplate-to-cell connection, at the top of the pedestal support at the baseplate connection, and at cell-to-cell connections. Bounding values of resultant loads are used to qualify the connections.

a. Baseplate-to-Rack Cell Welds

Reference [5.13] (ASME Code Section III, Subsection NF) permits, for Level A or B conditions, an allowable weld stress $\tau = .3 * (66,200) = 19,860$ psi. As stated in Subsection 5.5.3 (part ii) the allowable for Level D is 0.54 S_u, giving an allowable of 35,748 psi.

Weld stresses are determined through the use of a simple conversion factor (based on area ratios) applied to the corresponding stress factor in the adjacent rack material. The conversion factor is developed from the differences in base material thickness and length versus weld throat dimension and length as follows:

$$\frac{0.075*(8.8+0.075)}{0.0625*0.7071*6.0} = 2.51$$

where

0.075	is the cell wall thickness
8.8+0.075	is the mean box dimension
0.0625*0.7071	is the box-baseplate fillet weld throat size
6.0	is the length of the weld

The highest predicted cell to baseplate weld stress is calculated based on the highest R2, R6, and R7 values for the rack cell region (refer to Subsection 5.5.3.1 for definition of R2, R6, and R7 factors). These cell wall stress factors are converted into weld stress values as follows:

For SSE Simulation

$$\{[R6 * (1.2)]^2 + [R2 * (0.72)]^2 + [R7 * (0.72)]^2\}^{1/2} * S_y * \text{Ratio}$$
$$= \{[0.367 * (1.2)]^2 + [0.059* (0.72)]^2 + [0.052 * (0.72)]^2\}^{1/2} * (21,300) * 2.51$$
$$= 23,731 \text{ psi}$$

For OBE Simulation

$$\{[R6 * (0.6)]^2 + [R2 * (0.4)]^2 + [R7 * (0.4)]^2\}^{1/2} * S_y * \text{Ratio}$$
$$= \{[0.563 * (0.6)]^2 + [0.102 * (0.4)]^2 + [0.094* (0.4)]^2\}^{1/2} * (21{,}300) * 2.51$$
$$= 18{,}301 \text{ psi}$$

Since the calculated stress values are less than the corresponding allowable weld stresses, all welds between the baseplate and cell wall base are acceptable.

b. Baseplate-to-Pedestal Welds

The weld between baseplate and support pedestal is checked using finite element analysis to determine that the maximum stress is 15,860 psi for a ¼" fillet weld under a Level D event. This calculated stress value is conservatively compared with the Level A allowable of 19,860 psi.

c. Cell-to-Cell Welds

Cell-to-cell connections are by a series of connecting welds along the cell height. Stresses in storage cell to cell welds develop due to fuel assembly impacts with the cell wall. These weld stresses are conservatively considered by assuming that fuel assemblies in adjacent cells are moving out of phase with one another so that impact loads in two adjacent cells are in opposite directions and are applied simultaneously. This load application tends to separate the two cells from each other at the weld. In addition the cell-to-cell welds experience flexural shear loads due to bending of the rack cell structure. An evaluation of the SSE loads shows that the computed weld stress of 6,756 psi is less than the Level A allowable weld shear stress value of 19,860 psi. It is therefore concluded that the cell-to-cell welds and the adjacent materials are acceptable under all cases considered.

5.6.8 Dead Load Evaluation

The dead weight per pedestal for the heaviest loaded rack is 61,910 lbs, which is very low compared to an SSE load of 326,000 lbs. Since the Level A loads are approximately 20% of the Level D loads, while the Level A limits are approximately 50% of the Level D limits, the SSE load condition bounds the dead load condition and no further evaluation is performed for dead load only.

5.6.9 Assessment of Rack Fatigue Margin

Alternating stresses in metals produce metal fatigue if the amplitude of the stress cycles is sufficiently large. In high-density racks designed for sites with moderate to high postulated seismic action, the stress intensity amplitudes frequently reach values above the material endurance limit, leading to expenditure of the fatigue "usage" reserve in the material.

Because the locations of maximum stress (viz., the pedestal/rack baseplate junction) and the close placement of racks, a post-earthquake inspection of the high stressed regions in the racks is not feasible. Therefore, the racks must be engineered to withstand multiple earthquakes without reliance of nondestructive inspections for post-earthquake integrity assessment. ASME subsection NF does not require a fatigue evaluation for Class 3 linear-type supports, which is the applicable code for rack design. However, for conservatism, a fatigue life evaluation has been performed for the racks. The time-history method of analysis, deployed in this report, provides the means to obtain a complete cycle history of the stress intensities in the highly stressed regions of the rack. Having determined the amplitude of the stress intensity cycles and their number, the cumulative damage factor, U, can be determined using the classical Miner's rule:

$$U = \Sigma \frac{n_i}{N_i}$$

where n_i is the number of stress intensity cycles of amplitude σ_i, and N_i is the permissible number of cycles corresponding to σ_i from the ASME fatigue curve for the material of construction. U must be less than or equal to 1.0.

The cumulative damage factor for 1 SSE and 5 OBE events is determined as 0.615, which is well below the ASME Code limit of 1.0.

5.6.10 Local Stress Considerations

This section presents the results of evaluations for the possibility of cell wall buckling and the thermal stresses produced by an isolated hot cell.

5.6.10.1 Cell Wall Buckling

The allowable local buckling stresses in the fuel cell walls is obtained by using classical plate buckling analysis as taken from Section 9.2 of Reference [5.15]. The resulting local buckling stress limit of 15,928 psi is not violated anywhere in the body of the rack modules, since the maximum compressive stress in the outermost cell is

SSE: $\sigma = (1.2)(21{,}300) * R6$ (which is 0.367) = 9,380.5 psi

OBE: $\sigma = (0.6)(21{,}300) * R6$ (which is 0.563) = 7,195.2 psi

5.6.10.2 Analysis of Welded Joints in Rack

Cell-to cell welded joints are examined in this subsection under the loading conditions arising from thermal effects due to an isolated hot cell. This secondary stress condition is conservatively combined with primary stresses from other load conditions to demonstrate compliance with Ref. [5.2].

A thermal gradient between cells will develop when an isolated storage location contains a fuel assembly emitting maximum postulated heat, while the surrounding locations are empty. A conservative estimate of weld stresses along the length of an isolated hot cell can be obtained by considering a beam strip uniformly heated by 50°F, which is restrained from growth along one long edge. This thermal gradient is based on the results of the thermal-hydraulic analysis, which shows that the difference between the local cell maximum temperature and the bulk pool temperature is less than this value (actual temperature difference is less than 40°F per Chapter 6 results).

Using shear beam theory and subjecting the strip to a uniform temperature rise $\Delta T = 50°F$, one can calculate an estimate of the maximum value of the average shear stress in the strip. The strip is subjected to the following boundary conditions.

a. Displacement $U_x(x,y) = 0$ at $x = 0$, at $y = H/2$, for all x.

b. Average force $N_x(x) = 0$ at $x = L$

The final result for wall shear stress, maximum at $x = L$, is found to be given as

$$\tau_{max} = \frac{E\alpha\Delta T}{0.931}$$

where $E = 27.6 \times 10^6$ psi, $\alpha = 9.5 \times 10^{-6}$ in/in °F and $\Delta T = 50°F$.

Therefore, the maximum weld shear stress in an isolated hot cell, due to thermal gradient, is

$$\tau_{max} = 14{,}082 \text{ psi}$$

Under seismic conditions, the cell-to-cell welds also develop stress due to the flexural behavior of the rack cell structure and the fuel-to-cell wall impact forces. The maximum shear stress in the cell-to-cell welds due to seismic loading is 6,756 psi, which is reported in Subsection 5.6.7. When these two stress results are conservatively summed, the combined stress on the weld is still less than the minimum acceptance limit specified in Ref. [5.2] (i.e., 1.5 times normal limits or the lesser of 2Sy and Su). The normal (Level A) stress limit for a weld is 0.3 × Su per ASME Code Subsection NF. Thus, in accordance with Ref. [5.2], the applicable weld stress limit for evaluating thermal plus seismic stresses is 0.45 × Su. For SA-240 304 material at 200°F, 0.45 × Su is equal to 29,790 psi, which is greater than the combined weld stress of 20,838 psi (= 14,082 psi + 6,756 psi). Therefore, the combined shear stress in the cell-to-cell welds resulting from the load combination D + L + Ta + E' is less than the most restrictive acceptance limit provided in the 1978 OT position paper (GL 78-11) for thermal load combinations (i.e., "1.5 times normal limits").

To prove that the cell-to-cell welds are indeed the limiting rack component under thermal loading conditions, a 3-D finite element model of the largest spent fuel rack has been developed using ANSYS, and the thermal stresses throughout the entire rack have been solved for a bounding temperature distribution. The finite element solution confirms that the highest stressed region coincides with the cell-to-cell welds near the top of the rack where the temperature gradient between neighboring cells is at its maximum. More importantly the thermal stresses in the rack are within the acceptance limits provided in the OT position paper and Appendix D to SRP 3.8.4 for all load combinations involving temperature loadings.

The ANSYS finite element model used to solve the thermal stress distribution is shown in Figure 5.8. The model accurately reflects the size and dimensions of rack D4, which is the largest of the proposed spent fuel racks for BVPS-2. The support pedestals and rack baseplate are modeled

using solid elements (SOLID45), and the cell structure, including the cell boxes, filler panels, and corner angles, are modeled using shell elements (SHELL63). The weld connections are modeled in ANSYS by coupling lines of nodes between adjacent cells, between the baseplate and the cell walls, and between the baseplate and the support pedestals consistent with the rack design drawings. The bottom surfaces of the support pedestals are fixed in the vertical direction. Finally, a constant coefficient of thermal expansion of 8.9×10^{-6} in/in-°F is assigned to all elements in the ANSYS model. This input value conservatively bounds the mean coefficient of thermal expansion for SA-240 304L in going from 70°F to 200°F per Section II, Part D of the ASME Code.

To maximize the temperature gradient across the rack, the thermal stress analysis is performed assuming that half of the rack is loaded with freshly discharged fuel, and the other half is empty. The nodal temperatures applied to each of the cells in the loaded region of the rack are determined from the CFD analysis of SFP local water temperatures, which is discussed in Section 6.7. From the CFD solution, the variation in the SFP water temperature in the vertical direction, inside the hottest cell location, is plotted in Figure 5.9. For the thermal stress analysis using ANSYS, the temperature profile in Figure 5.9 is applied to each storage cell in the loaded region of the rack. Within the empty region of the rack, each node is assigned a temperature of 169.93°F, which is equal to the calculated SFP bulk water temperature following a normal full core offload. The applied temperature distribution for the thermal stress analysis is plotted in Figure 5.10 for the entire rack. The reference temperature used in ANSYS for thermal growth calculations is set to 70°F.

The resulting stress intensity distribution in the rack is plotted in Figure 5.11. The thermal stresses in the rack are negligible everywhere, except for at the boundary between the loaded and empty regions of the rack. The abrupt change in temperature across this boundary produces shear stresses in the cell-to-cell welds and tensile/compressive stresses in the adjoining cell walls. From the ANSYS solution, the maximum resultant force acting on a single cell-to-cell weld is found to be 2,557 lbf, and therefore the maximum shear stress in a single cell-to-cell weld (which is conservatively treated as a 6-inch long, 1/16" fillet weld) is 9,644 psi. This stress is

less than the weld stress (14,082 psi) estimated above, and therefore the previous calculation is conservative.

With respect to the cell base metal material, the maximum calculated stress intensity anywhere in the rack structure due to the abnormal thermal load (Ta) is 10,209 psi (see Figure 5.11). Conversely, for the non-thermal loads (i.e., D + L + E or E'), the maximum stress occurs at the base of the perimeter cells since the cell structure above the base plate acts like a cantilevered beam under horizontal seismic loading. From Section 5.6.10.1, the maximum combined flexure plus tensile/compressive stress due to SSE loading (D + L + E') is 9,381 psi. Notwithstanding the fact that the maximum thermal and seismic stresses occur at opposite ends of the rack, if the two maximums are summed together, the result is 19,590 psi, which is less than the yield strength of SA-240 304L material at 200°F (21,300 psi). Per the January 18th, 1979 amendment to the OT position paper [5.2], the acceptance limit for load combinations involving thermal loads is the "lesser of 2Sy or Su". For SA-240 304L, 2Sy (42.6 ksi) is less than Su (66.2 ksi); therefore, the acceptance limit is 2 x 21,300 psi = 42,600 psi. Since this value is more than two times the maximum combined thermal plus seismic stress (19,590 psi), the calculated stresses in the proposed spent fuel racks for BVPS-2 comply with the acceptance limit provided in the OT position paper (including the January 18th, 1979 amendment thereto). The preceding evaluation bounds all load combinations involving thermal loads from the OT position paper since it conservatively combines the seismic stresses due to SSE loading (E') with the thermal stresses due to an abnormal full core offload (Ta), and it compares the result with the acceptance limit for non-faulted conditions (i.e., "lesser of 2Sy or Su").

Appendix D to SRP 3.8.4 invokes the stress limits of the ASME Code, Section III, Subsection NF for Class 3 component supports for spent fuel rack design. Per Subparagraph NF-3121.11, thermal stresses need not be evaluated under Subsection NF. Nevertheless, the maximum combined thermal plus seismic stress of 19,590 psi (which is determined above) is less than faulted condition limit of 1.2Sy (= 25,560 psi) for combined flexure and axial loads per NF-3322.1 and F-1334. Under OBE load conditions (D + L + E), the maximum extreme fiber stress at the base of the rack cell structure is 7,195 psi. From Figure 5.11, the thermal stress near the

base of the rack due to an abnormal full core offload (Ta) is less than 5,000 psi. Accordingly, the maximum combined thermal plus seismic stress due to OBE is less than 12,195 psi. Therefore, even though it is not a Subsection NF requirement, the maximum combined thermal plus seismic stress due to OBE (< 12,195 psi) is less than the normal (Level A) condition limit for combined flexure and axial loads of 0.6Sy (= 12,780 psi) per NF-3322.1.

To conclude, the thermal stress analysis performed using ANSYS shows that the enveloping condition for the proposed rack design is the shear stress in the cell-to-cell welds. The maximum shear stress in the cell-to-cell weld, as predicted by ANSYS, is bounded by the result obtained using the beam strip model. With regard to the cell base metal, the maximum combined stress in the cell wall remains below the yield strength of the material even when maximum thermal and seismic stresses are summed together irrespective of their locations. This provides a safety factor greater than 2 when compared against the acceptance limit from the OT position paper (including the January 18th, 1979 amendment thereto) for load combinations involving thermal loads. Additionally, the maximum combined thermal plus seismic stresses in the rack cell structure are less than the ASME Subsection NF stress limits.

5.7 Cask Pit Rack Platform Analysis

A Cask Pit Rack Platform has been designed to provide a stable support for a loaded spent fuel storage rack in the cask pit at BVPS Unit No. 2. The platform is designed to rest on the pool floor and to support the rack from below. The platform consists of four tubular members, one beneath each rack support pedestal, with intervening cross-braces to prevent the platform from "rocking".

As stated in Section 5.5.4, a single rack analysis is performed in order to evaluate the seismic loads induced by a single rack on the supporting Cask Pit Rack Platform. These loads were used to evaluate the structural integrity of the platform using the ASME Section III, Subsection NF code allowables. The coefficient of friction at the interface between the rack support pedestals and the platform is based on a Gaussian distribution with a mean value of 0.5 and upper and lower bound values of 0.8 and 0.2, respectively. A finite element model of the platform was

developed using the ANSYS computer code. The pedestal loads calculated from the single rack analysis described in Section 5.5.4 were then applied to the platform to evaluate the stresses in the platform. For conservatism, the cask pit platform was assumed to be fixed to the floor for the ANSYS stress analysis. All safety factors were determined to be greater than 1.0. The minimum safety factor was calculated to be 1.27.

The maximum rack support pedestal displacement from the single rack run described in Section 5.5.4 is less than 0.5". The platform supports on which the rack support pedestals rest on are 12" x 12". The rack support pedestals are 4.5" in diameter. A displacement of less than 0.5" is insignificant, and will neither cause the rack to slide off the platform nor to tip over.

5.8 Bearing Pad Analysis

Bearing pads are placed between rack pedestals and the SFP floor to reduce the otherwise high stresses in the SFP concrete slab by spreading the concentrated load of each pedestal over a larger concrete contact area. This evaluation demonstrates that under maximum vertical forces in seismic events, the average compressive stress in the underlying concrete (calculated over the net bearing pad area) remains below the allowable value permitted by the American Concrete Institute, ACI 318-71 [5.20].

There are seven types of bearing pads, which are referred to as Types 1 through 7. Types 1, 5, 6 and 7 bearing pads are specially designed to be placed underneath the pedestals that are situated above leak chases in the concrete floor slab. These pads are designed to fit in the available space, and they are comprised of multiple plates stacked together to support either a single pedestal or a pair of closely spaced pedestals. The overall size of a Type 1 bearing pad assembly is 13" x 16" x 5.25" thick; a Type 5 bearing pad assembly is 11.5" x 22" x 5.25" thick; a Type 6 bearing pad assembly is 12" x 28" x 5.25" thick; a Type 7 bearing pad assembly is 15" x 23.5" x 5.25" thick.

Type 2 bearing pads are typical pads placed between the pedestals and the SFP liner above solid concrete away from leak chases. Each Type 2 bearing pad is a 12" x 12" x 2 ¾" thick plate, and it supports a single pedestal. Type 4 bearing pads (12" x 24" x 2 ¾") are twice the size of a Type 2 bearing so that they can support two closely spaced pedestals. Except for Type 3, all bearing pads rest directly on the SFP floor liner. Type 3 bearing pads, which measure 21" x 24" x 1" thick, are placed on the supporting steel blocks of the existing beam structures at the bottom of the SFP pool.

The BVPS Unit No. 2 SFP contains a series of beam structures supported by the pool floor. The existing racks are bolted to these beam structures. These beam structures are designed to carry the load of the existing racks and the stored fuel assemblies. The existing beam structures will not be removed from the SFP floor during this rerack. The new racks are designed such that the majority of the support pedestals are supported by the bearing pads placed directly on the underlying pool floor slab, except for three support pedestals which are supported by the existing beam structures using Type 3 bearing pads.

For each bearing pad type, the bearing stress in the underlying concrete is calculated by dividing the maximum pedestal load (including ACI load factors) by the net bearing pad area, which is defined as the total bearing pad area (i.e., pad length × pad width) minus the intersecting leak chase area beneath the bearing pad. The bearing pads adequately diffuse the peak pedestal load so that the compressive stress in the concrete slab is below the limit set by the governing concrete code [5.20] based on the design minimum concrete compressive strength of 3,000 psi. Also, for Type 3 bearing pads, the existing beam structure has been analyzed to determine that it can support the rack pedestal loads.

5.9 Interface Loads on Spent Fuel Pool Structure

The SFP at BVPS Unit No. 2 is a Safety Related, Seismic Category I, reinforced concrete structure. From the BVPS drawings it is noted that the BVPS Unit No. 2 SFP is the mirror reflection of the BVPS Unit No. 1 in terms of the storage locations (viz. the spent fuel storage area, the cask area and the fuel transfer canal) and the elevation of the slab and the confining walls.

Since a comprehensive evaluation of the pool structure was performed previously for the BVPS Unit No. 1 SFP in support of rerack license amendment application under NRC Docket No. 50-334, (Amendment No. 178 issued on November 1, 1993), the applicable loads (i.e. all Level A and Level D loads) and the capacities of both the BVPS Unit No. 1 and BVPS Unit No. 2 SFPs have been compared, and the key results for the BVPS Unit No. 2 SFP have been calculated using linear interpolation methodology.

The safety factor for the BVPS Unit No. 2 pool structure is determined by mixed interpolation, based on the increase (or decrease) in the load and the corresponding increase (or decrease) in the moment capacities for individual entities (walls and slab) of the pool structure, with the safety factor for the corresponding entity from BVPS Unit No. 1 SFP.

The structural evaluation of the BVPS-2 SFP concrete structure also includes the effects of the SFP liner heat-up. The thermal expansion of the SFP liner induces tensile loads in the walls since the liner is anchored to the concrete. The tensile load per unit width, F, induced in each SFP wall due to SFP liner heat-up is determined based on the following formula:

$$F = \frac{\alpha_s \Delta T_s - \alpha_c \Delta T_c}{\left(\frac{1}{E_s t_s} + \frac{1}{E_c t_c} \right)}$$

where α_s = coefficient of thermal expansion of Type 304 stainless steel (= 8.79 × 10^{-6} in/in-ΔºF);

α_c = coefficient of thermal expansion of concrete (= 5.5 × 10^{-6} in/in-ΔºF);

ΔT_s = temperature rise of SFP liner;

ΔT_c = temperature rise of concrete;

E_s = elastic modulus of Type 304 stainless steel (= 27.6 × 10^6 psi);

E_c = elastic modulus of concrete (psi) = $57{,}000\sqrt{f_c'}$;

f_c' = minimum compressive strength of concrete (= 3,000 psi);

t_s = thickness of SFP liner (= 0.25 in);

t_c = thickness of concrete wall;

For all SFP components except for the East-South and South-East Walls, the temperature rise of the SFP liner (ΔT_s) is taken as 100.3ºF, which is the difference between the SFP bulk water temperature following an abnormal full core offload (170.3ºF) and the stress-free temperature at the time of construction (which is assumed to be 70ºF). The East-South and South-East Walls, which separate the SFP from the transfer canal, are not governed by the abnormal full core offload condition. This is because during an offload the transfer canal is in communication with the SFP, and as a result the water temperature on both sides of the walls is roughly equal. The thermal gradients and the induced tensile loads in the East-South and South-East Walls are greatest during normal operating conditions when the transfer canal is drained. Thus, the tensile forces in the SFP walls and slab, as summarized in the table below, are the limiting results from either the abnormal thermal condition (Ta) or the normal operating thermal condition (To). Furthermore, the limiting results in the table below are conservatively used for all load combinations involving thermal loads, regardless of whether the load combination specifies To or Ta.

SFP Component	Concrete Wall Thickness, t_c (in)	Temperature Rise of SFP Liner, ΔT_s (Δ°F)	Temperature Rise of Concrete, ΔT_c (Δ°F)	Tensile Load per Unit Width, F (lbf/in)
West	72	100.3	56.0	3,840
North	90	100.3	24.6	5,026
South	88	100.3	52.7	3,983
East	24	100.3	70.4	3,124
East-South	54	85.3	55.3	2,954
South-East	48	85.3	56.2	2,907
Slab	120	100.3	33.5	4,725

The tensile loads summarized above have been included in the bending moment evaluation, as well as the one-way and two-way shear evaluations, for the SFP walls for the load combinations involving thermal loads (To, Ta). Specifically, for the one-way and two-way shear stress evaluations the permissible shear stress carried by the concrete has been computed for each SFP wall according to the interaction formula given in Section 11.4.4 of ACI 318-71 and the induced tensile load in each SFP wall (including the appropriate ACI load factors). Likewise, the bending moment capacities of the SFP walls have been adjusted according to the axial force-moment interaction diagrams for the SFP walls.

The safety factors against bending failure obtained for the BVPS Unit No. 2 SFP are shown in table below.

BVPS Unit No. 2 SFP Component (Wall / Slab)	**Minimum Safety Factor Against Bending Failure**
Slab	1.27
North Wall	1.79
East Wall	1.79
East-South Wall	1.21
South-East Wall	1.08
South Wall	1.31
West Wall	1.23

The safety factor is defined as the ratio of the moment capacity to the induced moment in the structure. All calculated safety factors must be shown to be above one to demonstrate the structural adequacy of the pool structure of the BVPS Unit No. 2 SFP.

The limiting results for the one-way shear evaluation of the BVPS Unit No. 2 SFP walls are summarized in the following table.

SFP Wall / Edge	Calculated Shear Stress (psi)	Permissible Shear Stress (psi)	Safety Factor
East / Vertical	59.44	62.20	1.05
West / Bottom	73.91	93.11	1.26
North / Bottom	52.40	93.11	1.78
South / Bottom	33.96	93.11	2.74

For the one-way shear evaluation, the total shear load on each wall is divided between the vertical edges and the bottom edge based on their tributary area.

The limiting results for the two-way shear evaluation of the BVPS Unit No. 2 SFP walls are summarized in the following table.

SFP Wall	Calculated Shear Stress (psi)	Permissible Shear Stress (psi)	Safety Factor
East	63.36	124.40	1.96
West	48.71	186.23	3.82
North	30.00	186.23	6.21
South	19.82	186.23	9.40

The two-way shear evaluation conservatively assumes that each wall is supported on only three sides (top edge is free). Accordingly, the shear capacity values in the above table are equal to the total sum capacity of the three-sided support perimeter of each wall evaluated at a distance d/2 from its perimeter edges (d is the distance from the extreme compression fiber to the center of the tension reinforcement).

The SFP reinforced concrete slab is 10-feet thick and founded on grade; therefore, a shear failure of the SFP slab is not limiting. The safety factors against shear failure for the East-South Wall and the South-East Wall are bounded by the safety factor for the East Wall in the above tables. This is because (a) the East-South Wall and the South-East Wall are at least two times thicker than the East Wall and (b) the wetted area of the East-South Wall and the South-East Wall are significantly less than the East Wall.

As shown in the tables above, all safety factors exceed the required minimum value of one. Therefore, it is concluded that the BVPS Unit No. 2 SFP structure is structurally adequate.

5.10 References

[5.1] USNRC NUREG-0800, Standard Review Plan, March 2007, (SRP 3.8.4 Rev. 2) and (SRP 3.7.1. Rev 3).

[5.2] (USNRC Office of Technology) "OT Position for Review and Acceptance of Spent Fuel Storage and Handling Applications", dated April 14, 1978, and January 18, 1979 amendment thereto (Generic Letter 78-11).

[5.3] Soler, A.I. and Singh, K.P., "Seismic Responses of Free Standing Fuel Rack Constructions to 3-D Motions", Nuclear Engineering and Design, Vol. 80, pp. 315-329 (1984).

[5.4] Soler, A.I. and Singh, K.P., "Some Results from Simultaneous Seismic Simulations of All Racks in a Fuel Pool", INNM Spent Fuel Management Seminar X, January, 1993.

[5.5] Singh, K.P. and Soler, A.I., "Seismic Qualification of Free Standing Nuclear Fuel Storage Racks - the Chin Shan Experience, Nuclear Engineering International, UK (March 1991).

[5.6] Holtec Computer Code MR216 (multi-rack transient analysis code, a.k.a. DYNARACK), Holtec Proprietary Report HI-961465 - WPMR Analysis User Manual for Pre&Post Processors & Solver, August 1997.

[5.7] Holtec Proprietary Report HI-89364 - Verification and User's Manual for Computer Code GENEQ, January 1990.

[5.8] Rabinowicz, E., "Friction Coefficients of Water Lubricated Stainless Steels for a Spent Fuel Rack Facility," MIT, a report for Boston Edison Company, 1976.

[5.9] Singh, K.P. and Soler, A.I., "Dynamic Coupling in a Closely Spaced Two-Body System Vibrating in Liquid Medium: The Case of Fuel Racks," 3rd International Conference on Nuclear Power Safety, Keswick, England, May 1982.

[5.10] Fritz, R.J., "The Effects of Liquids on the Dynamic Motions of Immersed Solids," Journal of Engineering for Industry, Trans. of the ASME, February 1972, pp 167-172.

[5.11] Levy, S. and Wilkinson, J.P.D., "The Component Element Method in Dynamics with Application to Earthquake and Vehicle Engineering," McGraw Hill, 1976.

[5.12] Paul, B., "Fluid Coupling in Fuel Racks: Correlation of Theory and Experiment", (Proprietary), NUSCO/Holtec Report HI-88243.

[5.13] ASME Boiler & Pressure Vessel Code, Section III, Subsection NF, 1998 Edition.

[5.14] ASME Boiler & Pressure Vessel Code, Section III, Appendices, 1998 Edition.

[5.15] Theory of Elastic Stability, Timoshenko and Gere, 2nd Edition, 1961, McGraw Hill.)

[5.16] ASME Boiler & Pressure Vessel Code, Section II, Part D, 1998 Edition.

[5.17] ACI 349-85, Code Requirements for Nuclear Safety Related Concrete Structures, American Concrete Institute, Detroit, Michigan.

[5.18] Not Used.

[5.19] "Nuclear Reactors and Earthquakes, U.S. Department of Commerce, National Bureau of Standards, National Technical Information Service, Springfield, Virginia (TID 7024).

[5.20] ACI 318-71, Building Code requirements for Structural Concrete," American Concrete Institute, Detroit, Michigan, 1971.

Table 5.4.1 PARTIAL LISTING OF FUEL RACK APPLICATIONS USING DYNARACK		
PLANT	DOCKET NUMBER(s)	YEAR
Enrico Fermi Unit 2	USNRC 50-341	1980
Quad Cities 1 & 2	USNRC 50-254, 50-265	1981
Rancho Seco	USNRC 50-312	1982
Grand Gulf Unit 1	USNRC 50-416	1984
Oyster Creek	USNRC 50-219	1984
Pilgrim	USNRC 50-293	1985
V.C. Summer	USNRC 50-395	1984
Diablo Canyon Units 1 & 2	USNRC 50-275, 50-323	1986
Byron Units 1 & 2	USNRC 50-454, 50-455	1987
Braidwood Units 1 & 2	USNRC 50-456, 50-457	1987
Vogtle Unit 2	USNRC 50-425	1988
St. Lucie Unit 1	USNRC 50-335	1987
Millstone Point Unit 1	USNRC 50-245	1989
Chinshan	Taiwan Power	1988
D.C. Cook Units 1 & 2	USNRC 50-315, 50-316	1992
Indian Point Unit 2	USNRC 50-247	1990
Three Mile Island Unit 1	USNRC 50-289	1991
James A. FitzPatrick	USNRC 50-333	1990
Shearon Harris Unit 2	USNRC 50-401	1991
Hope Creek	USNRC 50-354	1990
Kuosheng Units 1 & 2	Taiwan Power Company	1990
Ulchin Unit 2	Korea Electric Power Co.	1990
Laguna Verde Units 1 & 2	Comision Federal de Electricidad	1991
Zion Station Units 1 & 2	USNRC 50-295, 50-304	1992
Sequoyah	USNRC 50-327, 50-328	1992
LaSalle Unit 1	USNRC 50-373	1992
Duane Arnold Energy Center	USNRC 50-331	1992
Fort Calhoun	USNRC 50-285	1992
Nine Mile Point Unit 1	USNRC 50-220	1993

Table 5.4.1 (continued) PARTIAL LISTING OF FUEL RACK APPLICATIONS USING DYNARACK		
PLANT	DOCKET NUMBER(s)	YEAR
BVPS Unit No. 1	USNRC 50-334	1992
Salem Units 1 & 2	USNRC 50-272, 50-311	1993
Limerick	USNRC 50-352, 50-353	1994
Ulchin Unit 1	KINS	1995
Yonggwang Units 1 & 2	KINS	1996
Kori-4	KINS	1996
Connecticut Yankee	USNRC 50-213	1996
Angra Unit 1	Brazil	1996
Sizewell B	United Kingdom	1996
Waterford 3	USNRC 50-382	1997
J.A. Fitzpatrick	USNRC 50-333	1998
Callaway	USNRC 50-483	1998
Nine Mile Unit 1	USNRC 50-220	1998
Chin Shan	Taiwan Power Company	1998
Vermont Yankee	USNRC 50-271	1998
Millstone 3	USNRC 50-423	1998
Byron/Braidwood	USNRC 50-454, 50-455, 50-567, 50-457	1999
Wolf Creek	USNRC 50-482	1999
Plant Hatch Units 1 & 2	USNRC 50-321, 50-366	1999
Harris Pools C and D	USNRC 50-401	1999
Davis-Besse	USNRC 50-346	1999
Enrico Fermi Unit 2	USNRC 50-341	2000
Kewaunee	USNRC 50-305	2001
V.C. Summer	USNRC 50-395	2001
St. Lucie	USNRC 50-335, 50-389	2002
Turkey Point	USNRC 50-250, 251	2002
Clinton	USNRC 50-461	2003
Diablo Canyon Unit 1 & 2	USNRC 50-275, 50-323	2004
Cooper	USNRC 50-298	2006

Table 5.4.2

DEGREES-OF-FREEDOM

LOCATION (Node)	DISPLACEMENT			ROTATION		
	U_x	U_y	U_z	θ_x	θ_y	θ_z
1	p_1	p_2	p_3	q_4	q_5	q_6
2	p_7	p_8	p_9	q_{10}	q_{11}	q_{12}
Node 1 is attached to the rack at the bottom most point. Node 2 is attached to the rack at the top most point. Refer to Figure 5.1 for node identification.						
2*	p_{13}	p_{14}				
3*	p_{15}	p_{16}				
4*	p_{17}	p_{18}				
5*	p_{19}	p_{20}				
1*	p_{21}	p_{22}				

where the relative displacement variables q_i are defined as:

$p_i = q_i(t) + U_x(t)$ $\quad i = 1,7,13,15,17,19,21$

$= q_i(t) + U_y(t)$ $\quad i = 2,8,14,16,18,20,22$

$= q_i(t) + U_z(t)$ $\quad i = 3,9$

$= q_i(t)$ $\quad i = 4,5,6,10,11,12$

p_i denotes absolute displacement (or rotation) with respect to inertial space

q_i denotes relative displacement (or rotation) with respect to the floor slab

* denotes fuel mass nodes

U(t) are the three known earthquake displacements

Table 5.4.3 RACK MATERIAL DATA (200°F) (ASME - Section II, Part D)			
Material	Young's Modulus E (psi)	Yield Strength S_y (psi)	Ultimate Strength Su (psi)
SA240; 304L S.S.	27.6×10^6	21,300	66,200
SUPPORT MATERIAL DATA (200°F)			
SA240, Type 304 (upper part of support feet)	27.6×10^6	25,000	71,000
SA-564-630 (lower part of support feet; age hardened at 1100°F)	28.5×10^6	106,300	140,000

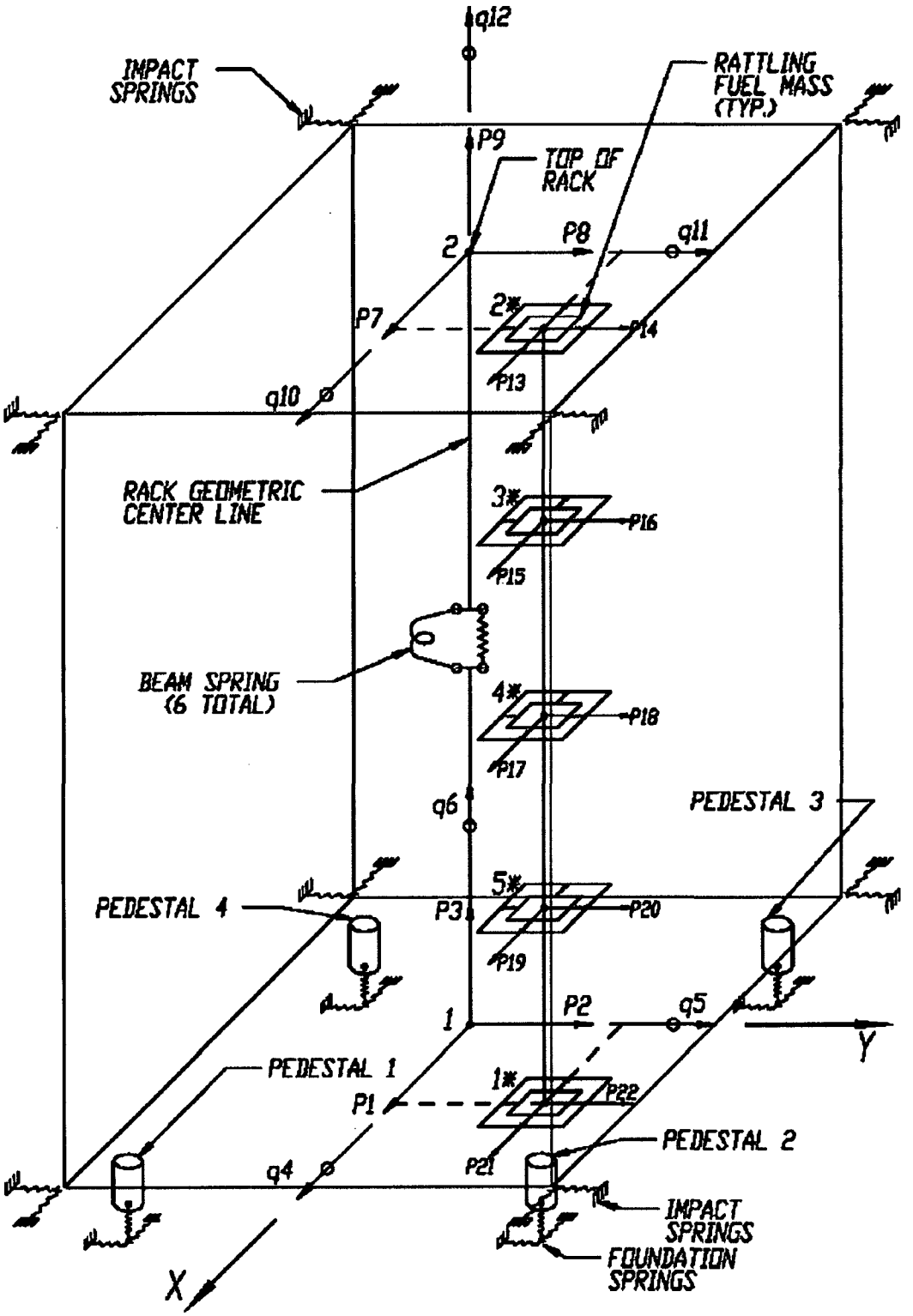

Figure 5.1: Single Rack Dynamic Model

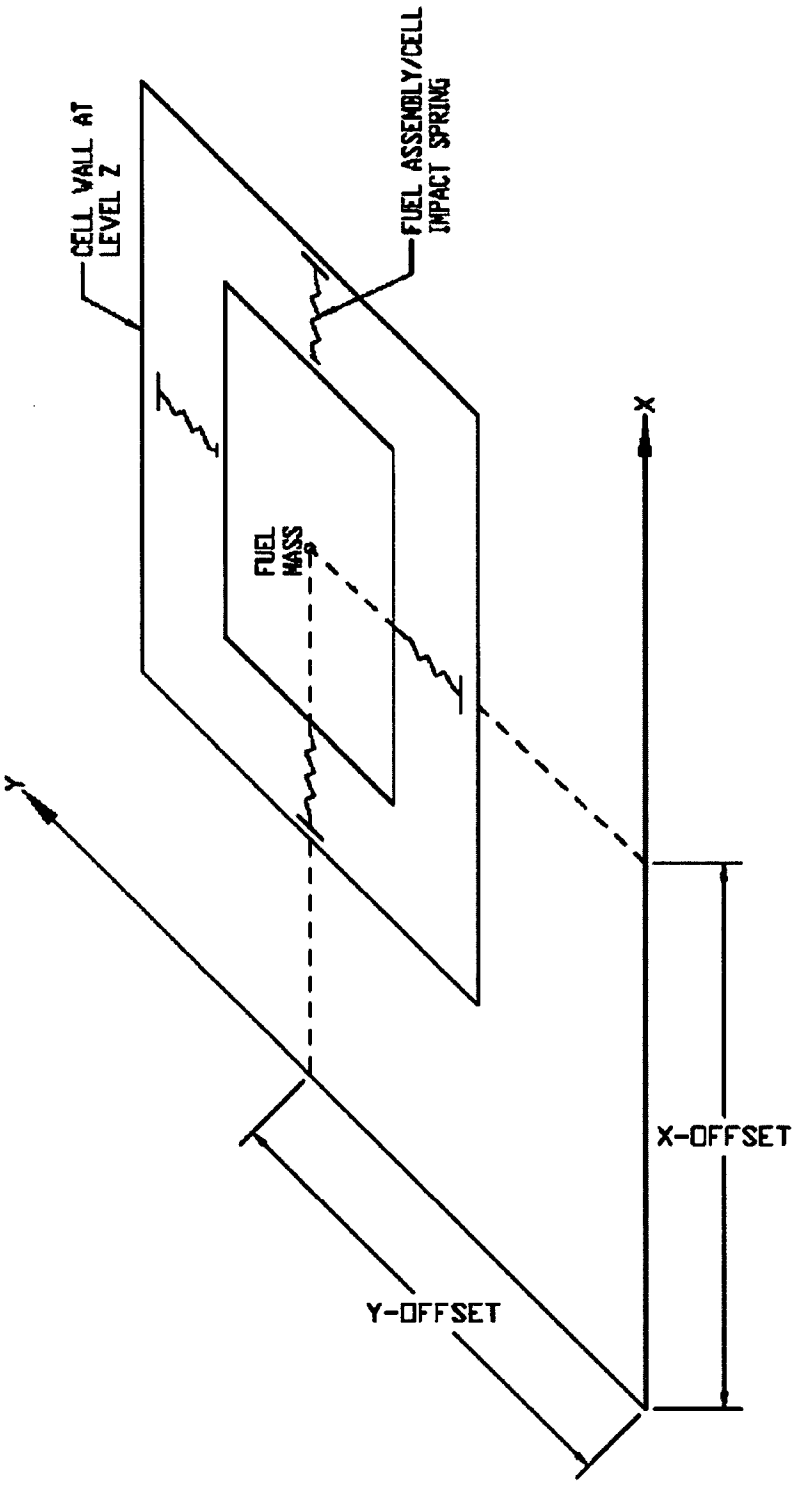

Figure 5.2: Fuel-to-Rack Impact Springs

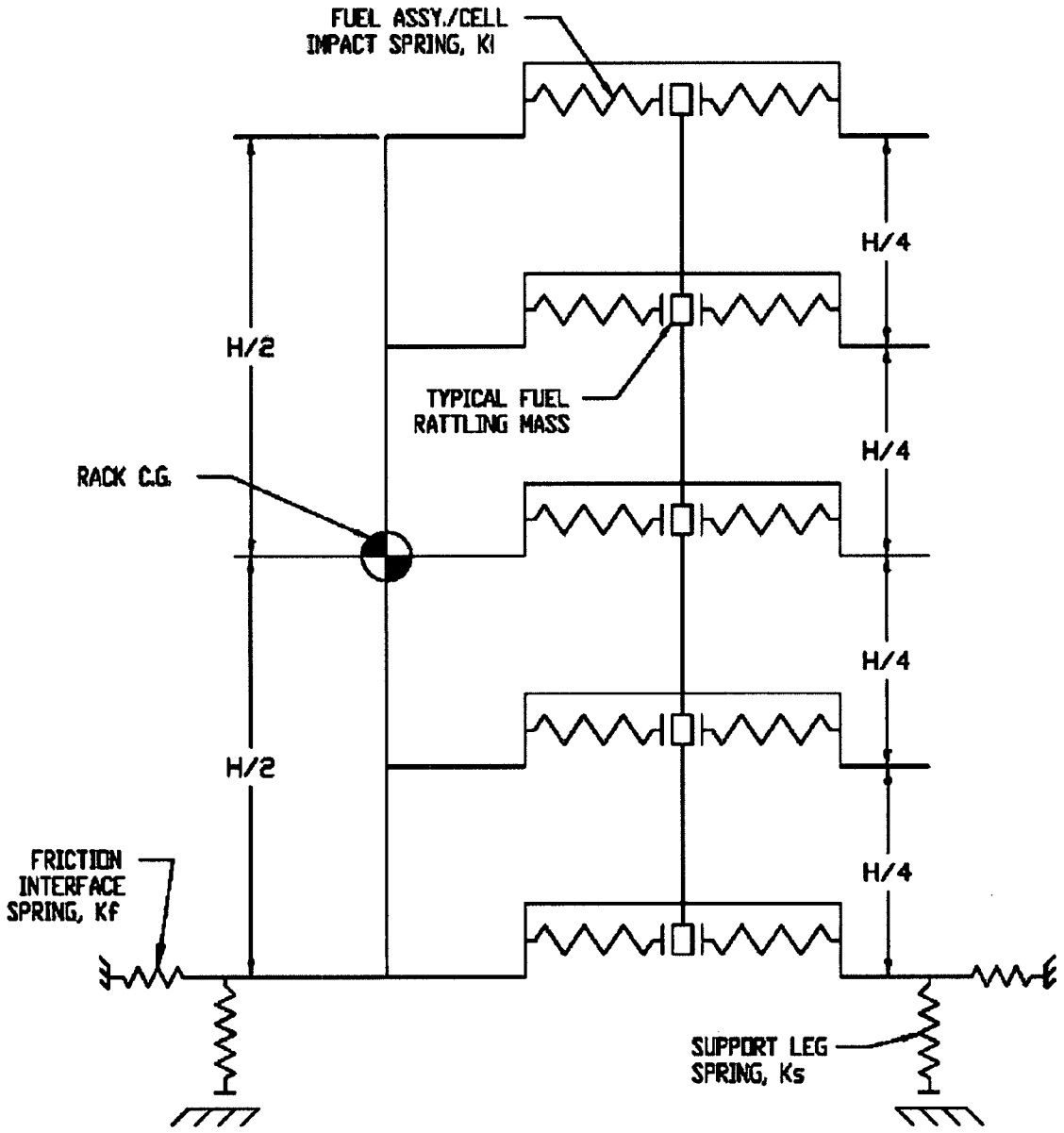

Figure 5.3: 2-D Schematic Elevation of the Storage Rack Model

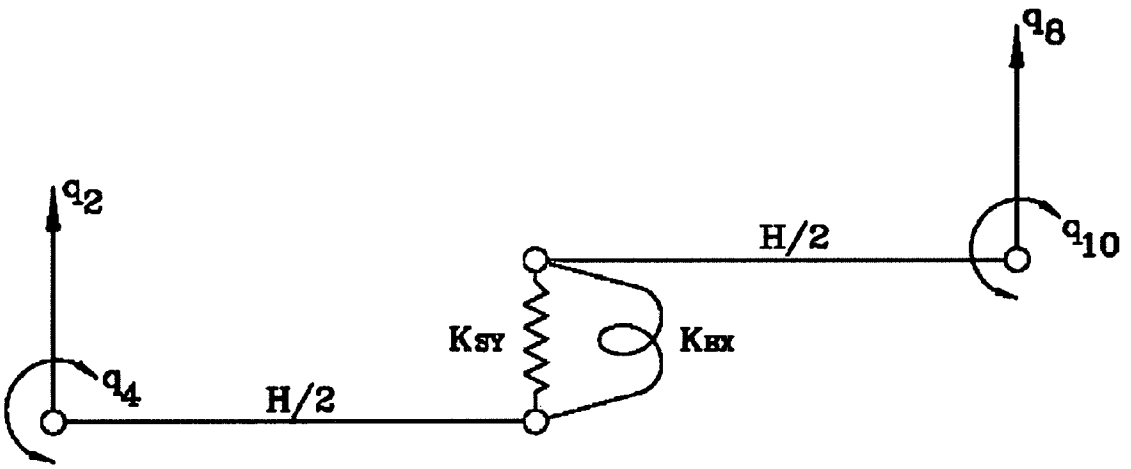

RACK DEGREES-OF-FREEDOM FOR Y-Z PLANE BENDING
WITH SHEAR AND BENDING SPRING

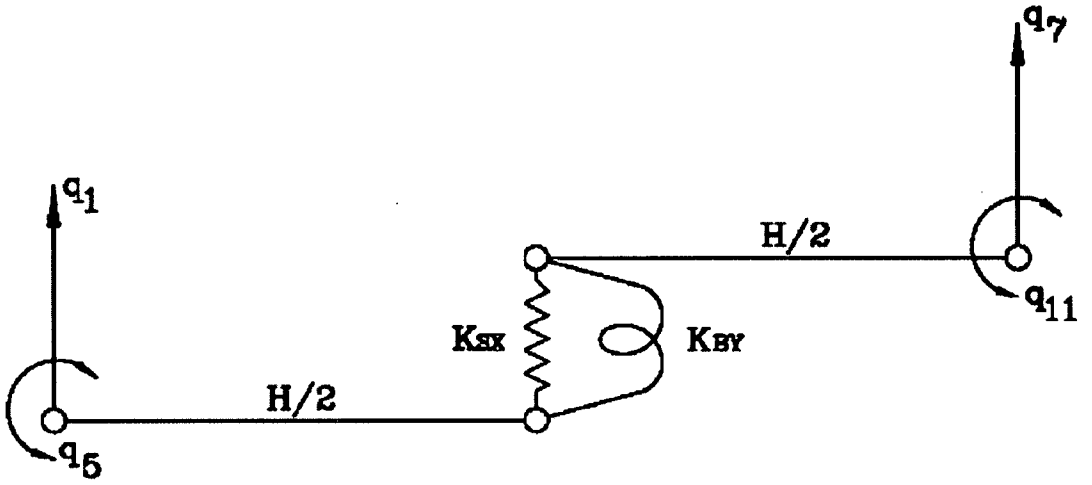

Figure 5.4: Rack Degrees of Freedom and Modeling Technique

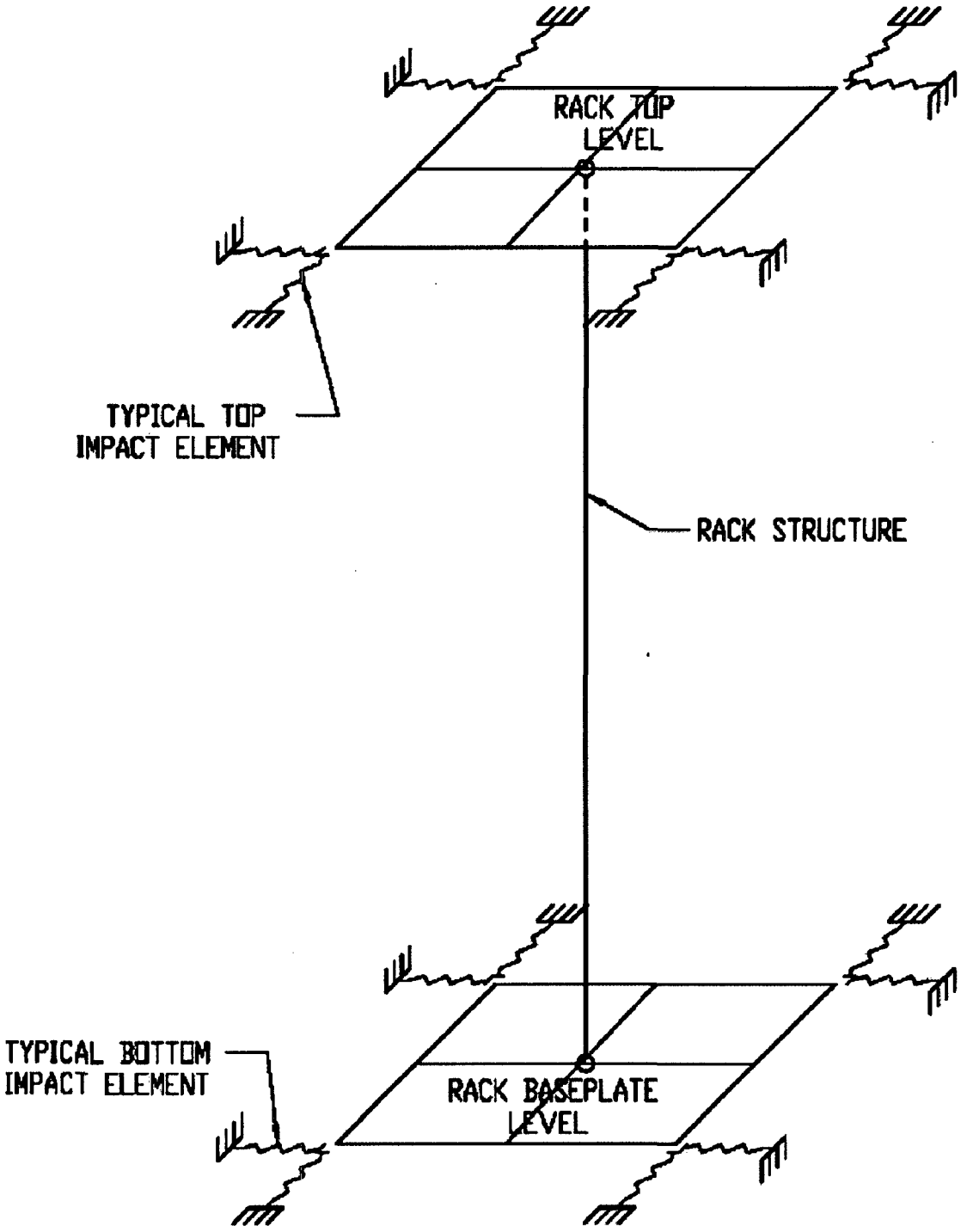

Figure 5.5: 2-D Inter-Rack Impact Springs

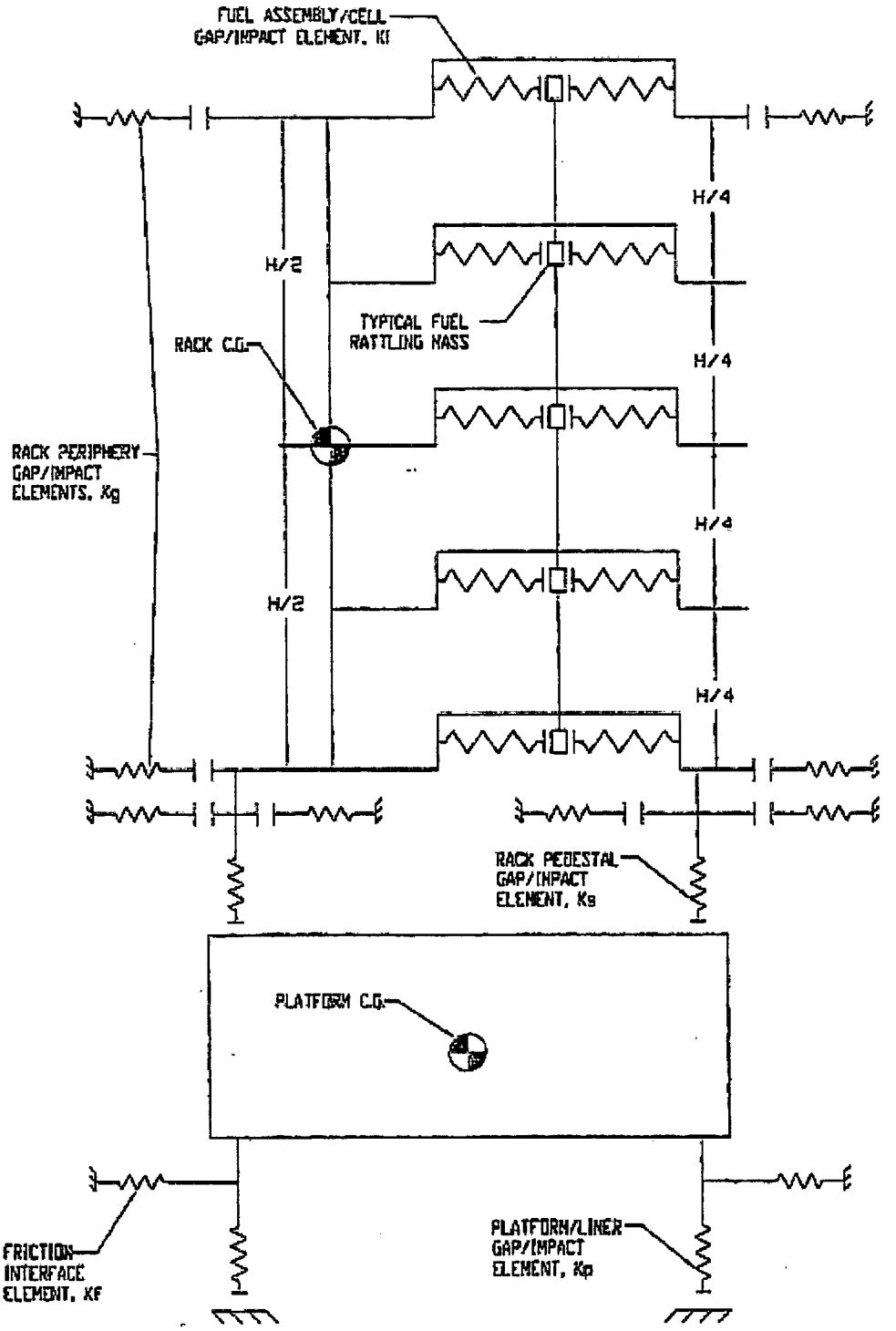

Figure 5.6: 2-D Schematic Elevation of the Coupled Rack-Platform Model

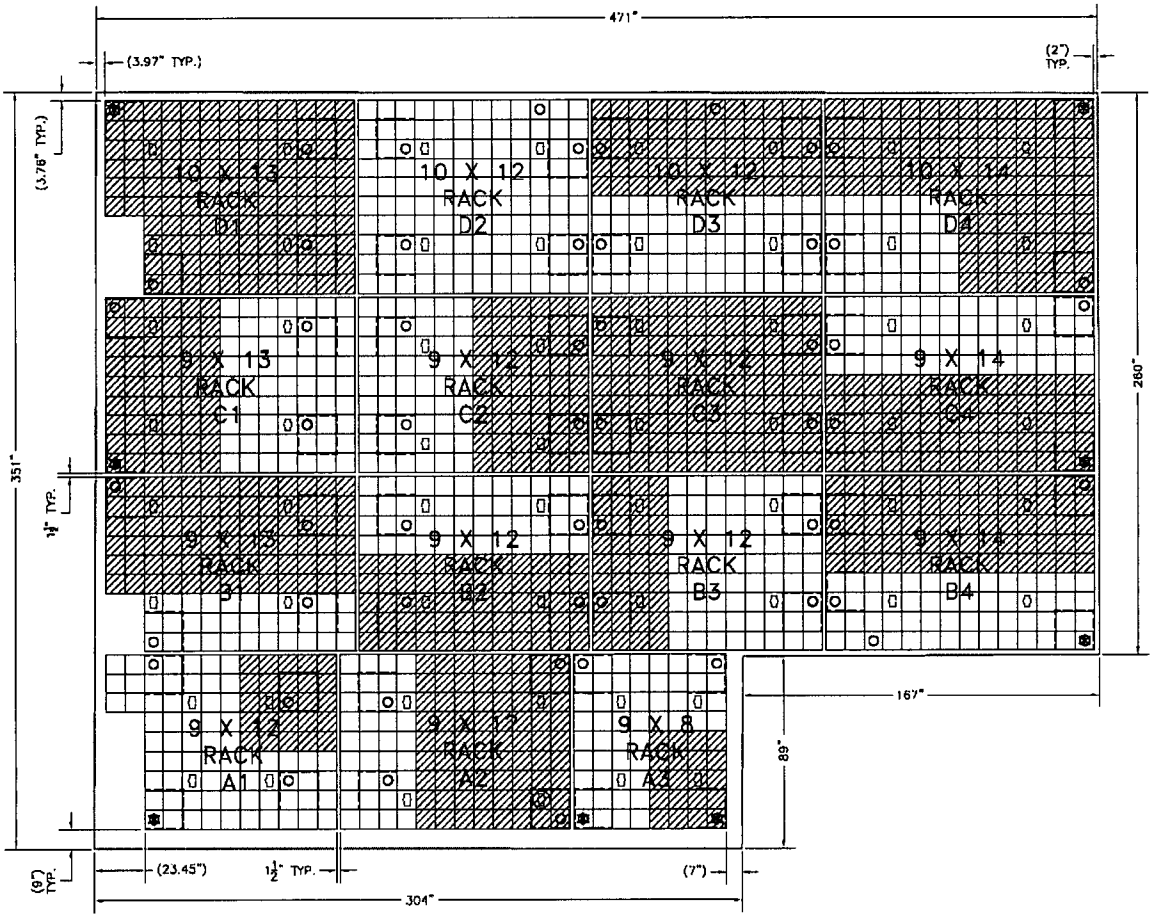

INTERIM FUEL LOADING CONDITION

Figure 5.7: Partially Loaded Rack Configuration

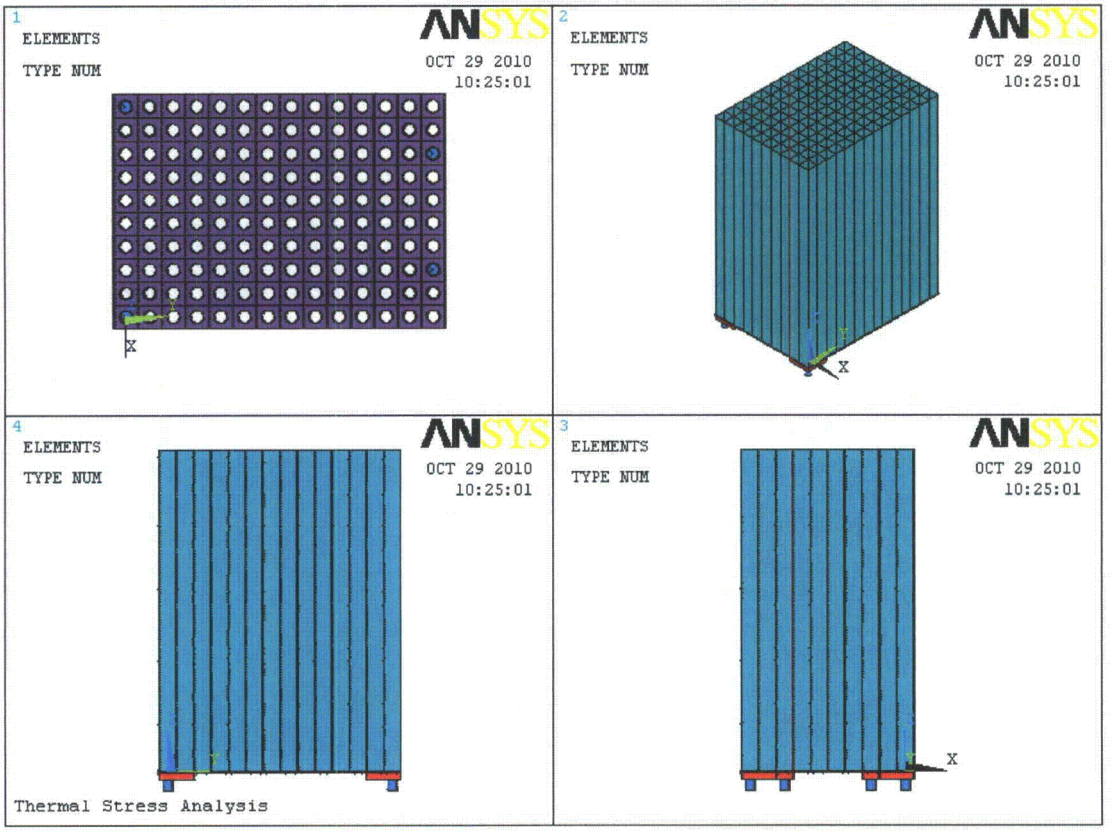

Figure 5.8: ANSYS Finite Element Model of Rack D4

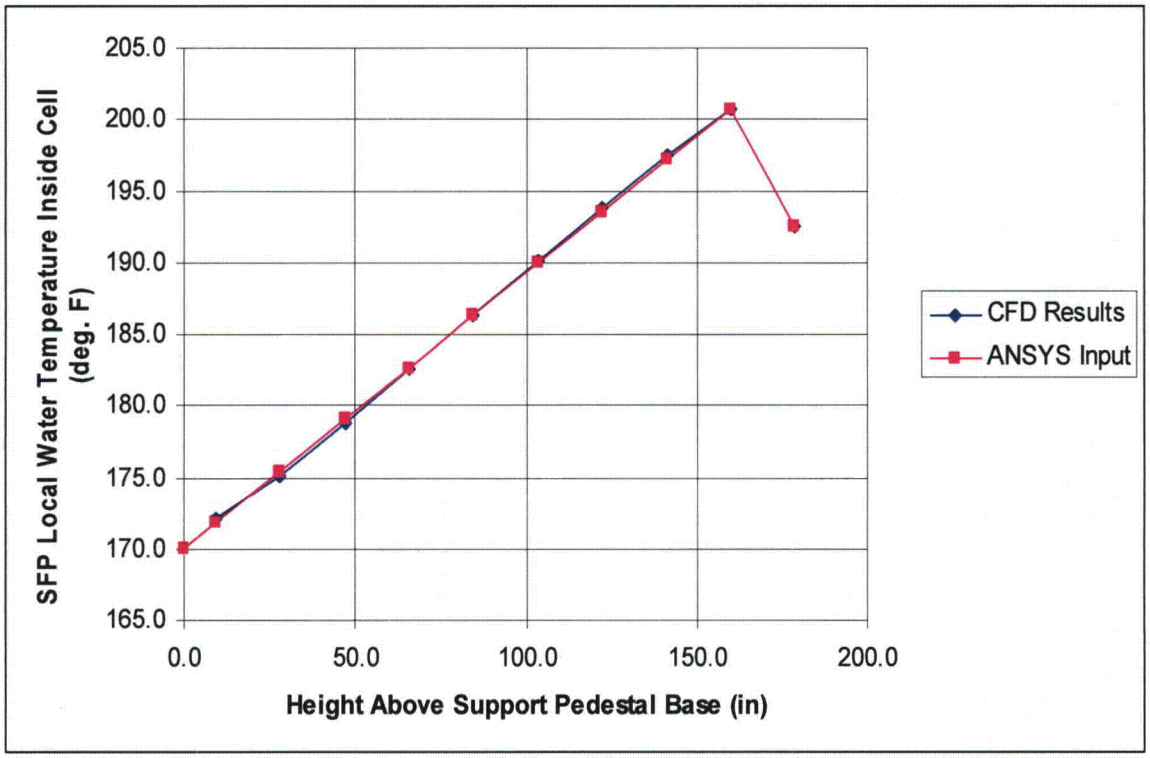

Figure 5.9: SFP Local Water Temperature Inside Hottest Cell Location Due to Abnormal Full Core Offload

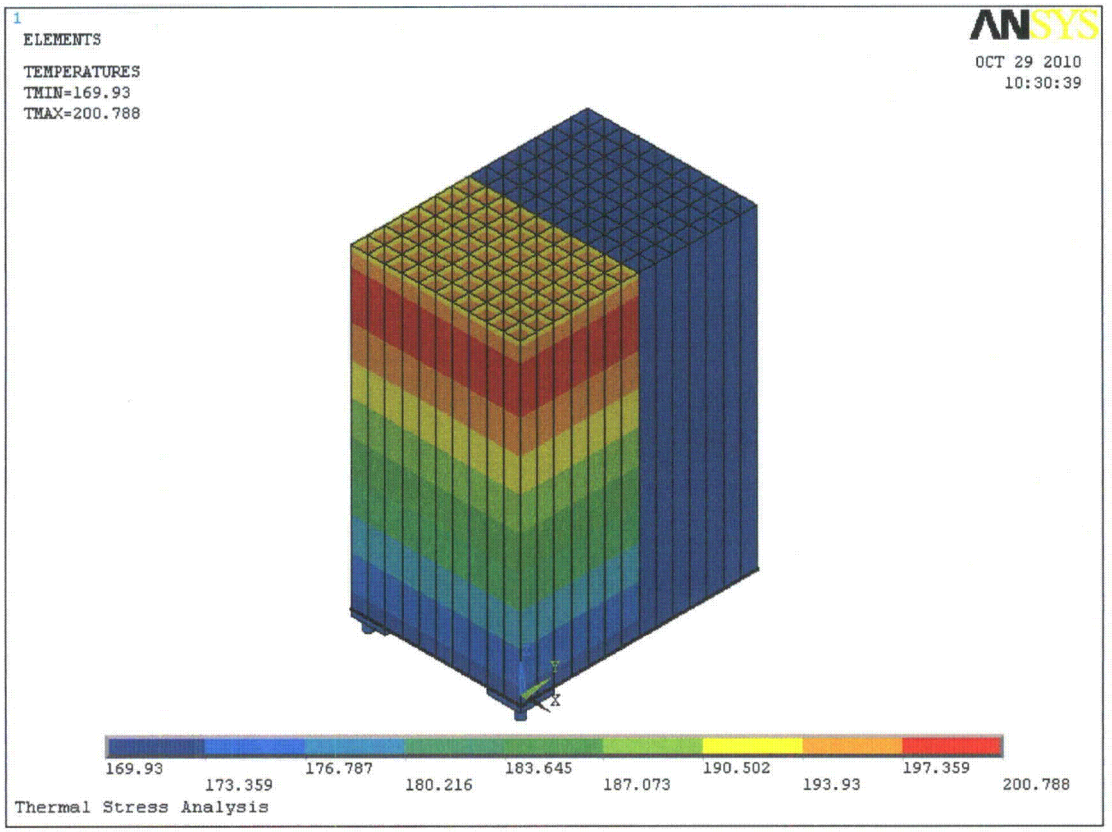

Figure 5.10: Applied Temperature Distribution for Thermal Stress Analysis

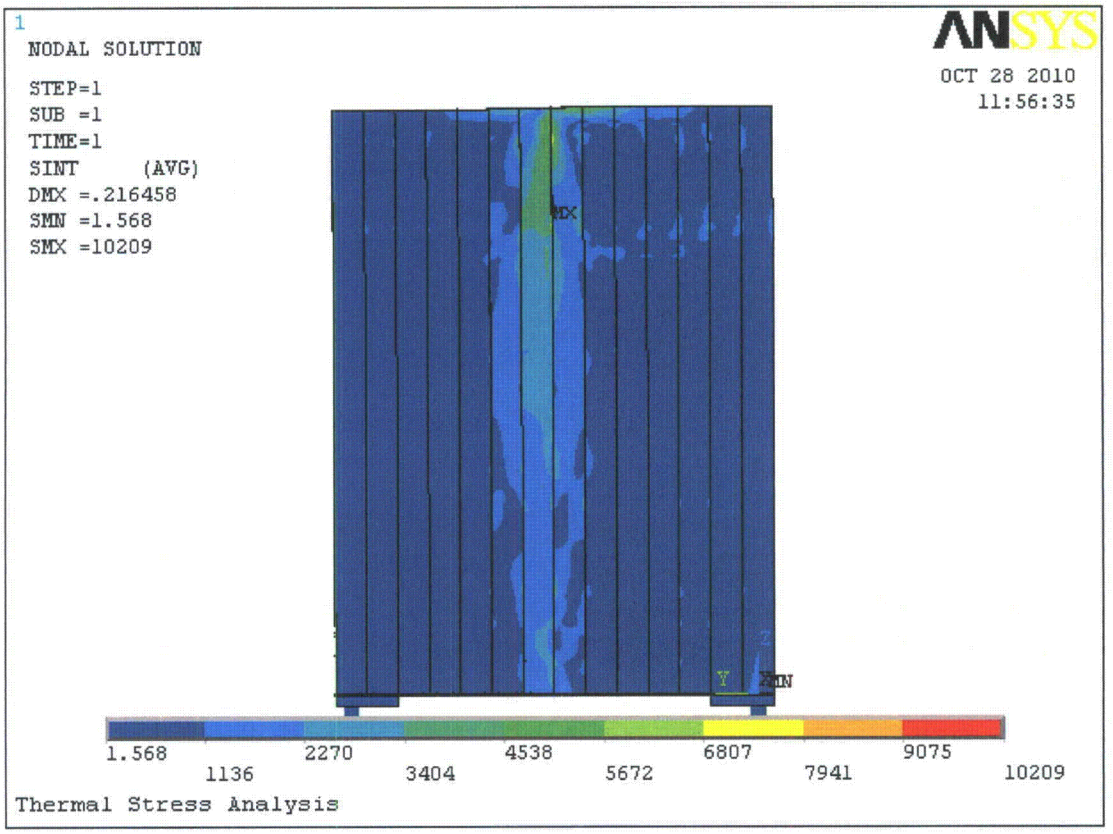

Figure 5.11: Thermal Stresses in the Rack Due to Abnormal Temperature Load (Ta)

7.0 MECHANICAL ACCIDENTS CONSIDERATIONS

7.1 Introduction

The USNRC OT position paper [7.1.1] specifies that the design of the rack must ensure the functional integrity of the spent fuel racks under all credible fuel assembly drop events.

This section contains synopses of the analyses carried out to demonstrate the regulatory compliance of the proposed racks under postulated accidental drop events [7.1.2] germane to the fuel pools; namely, that of a fuel assembly, a fuel rack and a gate.

7.2 Description of Mechanical Accidents

Several categories of accidental drop events are considered. Fuel drop evaluations are performed to evaluate the racks subsequent to a fuel assembly impact. The pool structure is evaluated for the drop of a fuel rack during installation. A pool gate drop is also evaluated to assess damage to the rack. Additionally, damage to the fuel assembly as a result of dropping of a fuel assembly on top of a stored fuel assembly in the rack is also considered and evaluated. Additional evaluations were also performed to consider the ability of the rack to withstand the uplift force from a stuck fuel assembly.

In the so-called "shallow" drop event, a fuel assembly, along with the portion of handling tool that is severable in the case of a single element failure, is assumed to drop vertically and hit the top of the rack. Additionally, a dropping of the pool gate is also postulated wherein the gate is assumed to be dropped over a rack to determine the extent of damage to the rack. Inasmuch as the new racks are of honeycomb construction, the deformation produced by the impact is expected to be confined to the region of collision. However, the "depth" of damage to the affected cell walls must be demonstrated to remain limited to the portion of the cell above the top of the "neutron absorber zone" which is defined as the vertical length of the cell blanketed by the fixed neutron absorber panel.

In order to utilize an upper bound of kinetic energy at impact, the impactor (fuel assembly including the handling tools) is conservatively assumed to weigh 2,450 lbs and the free-fall height is assumed to be 24 inches. Similarly, the pool gate weighing 4,020 lbs is assumed to free fall from the height of 24 inches.

The analysis of the shallow drop event considers two impact locations:

i) a vertical fuel assembly drop from a height of 24 inches above the rack onto a perimeter cell wall (see Figure 7.2.1);

ii) a vertical fuel assembly drop from a height of 24 inches above the rack onto an interior cell wall.

The second class of fuel drop event postulates that the impactor falls through an empty storage cell impacting the fuel assembly support surface (i.e., rack baseplate). This so-called "deep" drop event threatens the structural integrity of the baseplate. If the baseplate is pierced and the fuel assembly impacts the pool liner, then an abnormal condition may develop where the enriched zone of fuel assembly is outside the "poisoned" space of the fuel rack. To preclude damage to the pool liner and to avoid the potential of an abnormal fuel storage configuration in the aftermath of a deep drop event, it is required that the baseplate remain unpierced and that the maximum lowering of the baseplate is considered in the criticality evaluations.

The deep drop event can be classified into two scenarios, namely, a fuel drop through an interior cell away from the support pedestal (scenario 1), as shown in Figure 7.2.2, and a fuel drop through a cell located above a support pedestal (scenario 2), as shown in Figure 7.2.3. In deep drop scenario 1, the fuel assembly impacts the baseplate away from the support pedestal, where it is more flexible. Severing or large deflection of the baseplate leading to a secondary impact with the pool liner are unacceptable results. In deep drop scenario 2, the baseplate is buttressed by the support pedestal and presents a hardened impact surface, resulting in a high impact load. The principal design objective is to ensure that this accident does not compromise the structural integrity of the SFP floor liner.

In the third type of drop event, a rack is assumed to drop from the top water level in the pool and hits the pool floor, as shown in Figure 7.2.4. A representative model of the heaviest rack in the pool is used for the rack drop analysis. The structural integrity of the concrete floor must be demonstrated to be maintained in the rack drop event, and the effect on the liner plate is also evaluated. The acceptance criterion is that catastrophic pool structure damage, such that there is rapid loss of pool water inventory, is not allowed. In addition to the fuel and rack drops, the consequences of a potential gate drop onto the rack are also considered.

The last type of drop event is the postulated drop of a fuel assembly on top of a stored fuel assembly in the rack. The principal design objective is to ensure that this accident does not cause catastrophic damage (i.e. failure of all rods) to the fuel assembly.

In addition to the above drop events, the structural integrity of rack cell walls under the uplift load caused by a postulated stuck fuel assembly is also evaluated. The rack cell wall must be able to withstand this load without deforming the rack cell such that it does not adversely affect the integrity of the neutron absorber and thus affect the subcriticality of stored fuel array.

7.3 Incident Impact Velocity

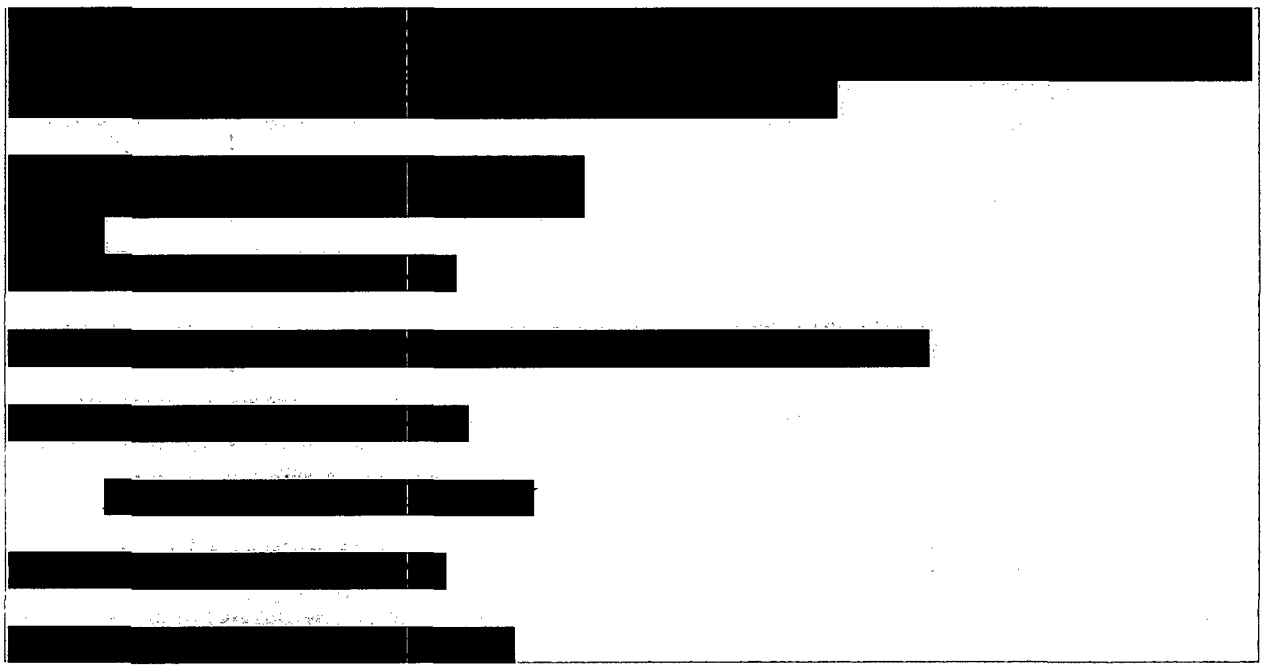

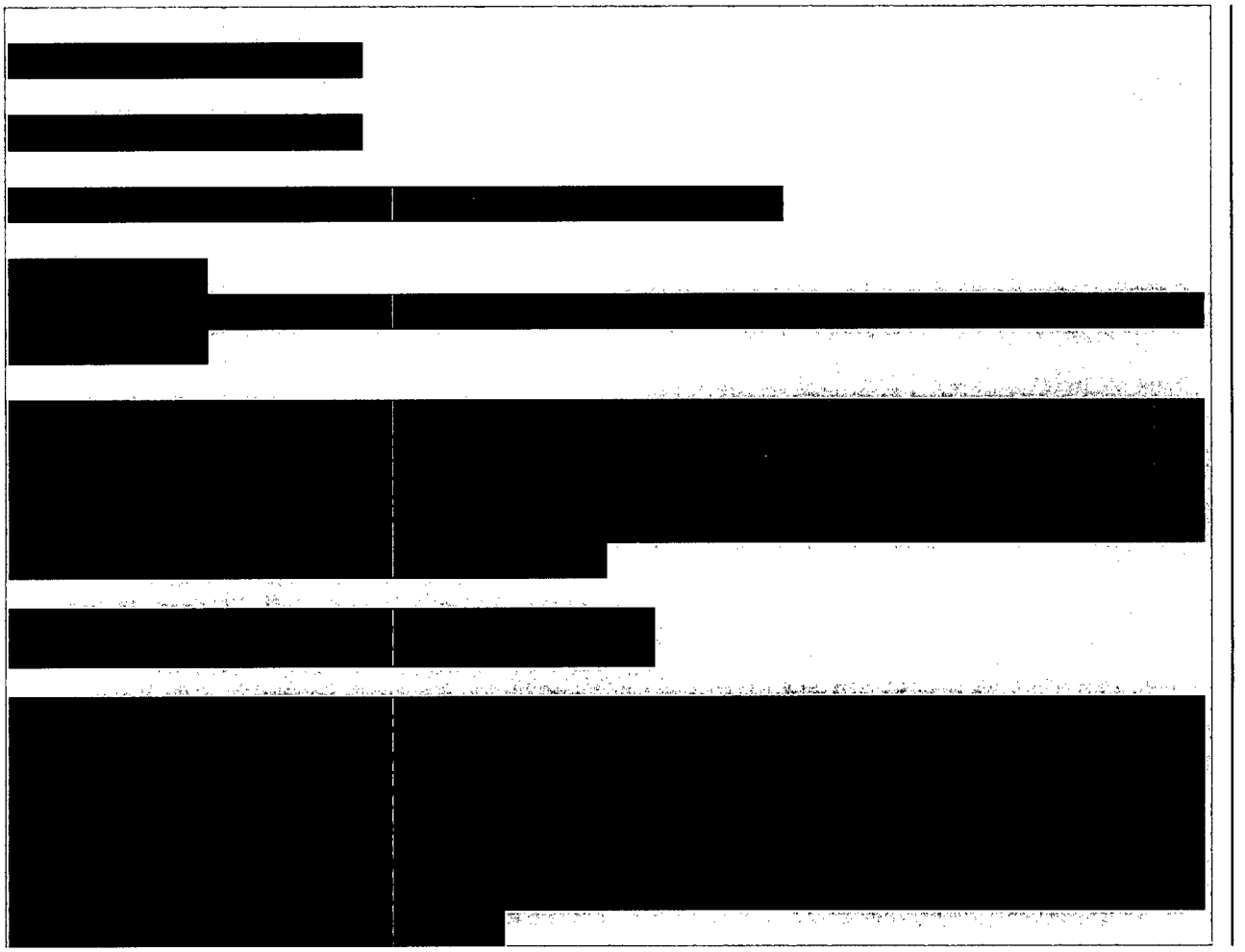

7.4 Mathematical Model

In the first step of the solution process, the velocity of the dropped object (impactor) is computed for the condition of underwater free fall in the manner of the formulation presented in the above section. Table 7.4.1 contains the computed velocities for the various drop events.

In the second step of the solution, an elasto-plastic finite element model for each drop event is prepared with the Holtec QA validated computer Code LS-DYNA. The model simulates the transient collision event with full consideration of plastic, large deformation, wave propagation, and elastic/plastic buckling modes.

In the "shallow" and the "deep" drop events, the fuel assembly is modeled by an equivalent

elasto-plastic rod with a concentrated mass (representing the handling tool) and a properly modeled rigid end-fitting at its two extremities. Shell elements are used to model the thin cell walls and weld connections. The rack baseplate is modeled with thick shell elements. Moreover, the rack support female block and pedestal are modeled with solid elements. Other structural components, such as the liner and concrete slab, are also properly modeled with elasto-plastic shell and solid elements in all drop events. Two models are developed to analyze the rack drop event. Based on engineering judgment that a rack drop accident will not cause a global structural failure of the SFP slab, a local model is developed based on a small region of the slab (55.25" long x 55.25" wide x 24" thick) to maximize the predicted local damage of the SFP floor. To obtain a quantitative assessment of the SFP slab global behavior, a global model that considers the entire SFP slab and the lower portion of the SFP walls is developed for evaluating both local and global responses of the impacted SFP slab. For the fuel-to-fuel impact drop event (for fuel damage evaluation), the fuel assembly's fuel rods and guide tubes are explicitly modeled using beam elements, and the rack is represented by a single storage cell (with its bottom end nodes fully constrained), which provides lateral supports to the deformed fuel rods. The physical properties of material types undergoing deformation in the postulated impact events are summarized in Table 7.4.2.

The base metal material (SA-240 304L) and the weld material (Type 308) are both modeled in LS-DYNA using material model MAT_024 (i.e., MAT_PIECEWISE_LINEAR_PLASTICITY). The true stress-strain curves are input as user-defined curves where the data points in the plastic deformation region are determined according to the following power law relationship:

$$\sigma = K\varepsilon^n$$

where σ = true stress

K = strength coefficient

ε = true strain

n = strain-hardening exponent

The methodology used to obtain the values of K and n, for a specific material, from a set of engineering stress-strain data (e.g., strength properties from ASME Section II, Part D) is

provided in Holtec Position Paper DS-307 [7.4.1]. Table 7.4.3 provides the values of K and n that are used to model the behavior of the base metal material and the weld material in the shallow drop analysis for the BVPS-2 spent fuel racks. Note that the yield strength, ultimate strength and Young's Modulus of the weld material are conservatively assumed to be identical to those of the base material, leading to an identical power law relationship for both materials (values of "K" and "n") as shown in Table 7.4.3.

The ultimate failure strain limits for the base metal material and the weld material are determined by multiplying the 98 percent exceedance uniaxial failure strains (which are derived from the reduction of area data provided in Table B.1 of NUREG-1864 [7.4.2]) by a triaxial factor of 0.5 (for biaxial tension). The resulting failure strain limits for the base metal material and the weld material are 0.362 and 0.246, respectively, which are input to LS-DYNA as constant value properties.

The strain rate amplification curve applied to the base metal material, which is obtained from [7.4.3], is shown in Figure 7.4.1. Throughout the simulation, the strain rate amplification factor for each base metal element is determined based on the instantaneous strain rate of the element. The time-dependent and element-dependent amplification factors are applied only to the stress values in the true stress-strain curve for the base metal material.

7.5 Results

7.5.1 Shallow Drop Event

The LS-DYNA analysis results for the fuel assembly drop onto a perimeter cell are shown in Figure 7.5.1 and summarized in Table 7.5.1. The results for the fuel assembly drop onto an interior cell are shown in Figure 7.5.2 and summarized in Table 7.5.2. The plastic deformation in the rack cell walls resulting from a shallow fuel drop accident (onto a perimeter cell or an interior cell) does not extend down into the "neutron absorber zone". For the BVPS-2 spent fuel racks the minimum distance from the top of the rack to the top edge of the neutron absorber panel (i.e., neutron absorber zone) is 19.75 inches. From the LS-DYNA simulations, the dropped fuel assembly moves downward crushing the impacted cell wall to a maximum depth of 3.15 inches (interior cell drop), and the plastic strain in the impacted cell wall diminishes to zero at a distance of 12 inches (perimeter cell drop) below the top of the rack (see Figure 7.5.1). Since the depth of damage by either measure is less than 19.75 inches, the neutron absorber panels do not suffer any damage, and therefore the shallow drop accident has no adverse effect on the criticality safety analysis for the BVPS-2 spent fuel racks. In fact, the criticality safety analysis takes no credit for the uppermost 1.3 inches of neutron absorber length, which extends above the active fuel region (assuming the maximum active fuel height and worst-case tolerances). Therefore, taking into consideration the criticality safety analysis, the more precise limit on the permanent deformation to the spent fuel rack due to a shallow drop accident is no greater than 21.05 inches (= 19.75 inches + 1.3 inches) measured from the top of the rack. Based on this criterion, the minimum computed safety factor for the shallow drop accident is:

$$SF = \frac{21.05"}{12"} = 1.75$$

The vertical gate drop accident will involve at least three rack cells because of the dimensions of the gate; a gate drop accident hitting only a periphery cell wall would lead to immediate gate rotation because the gate width is more than three times the size of the rack cell. However, the impact energy of the gate is only about 1.4 times that of the fuel assembly in the shallow drop event. Therefore, it can be concluded that the gate drop accident is bounded by the shallow drop event in terms of the depth of permanent deformation measured from the top of the rack.

7.5.2 Deep Drop Events

The deep drop scenario 1 (through an internal cell away from the support pedestal) does produce some deformation of the baseplate and localized severing of the baseplate/cell wall welds. Figure 7.5.3 shows the deformed baseplate configuration. However, the fuel assembly support surface is lowered by less than 2 inches, which is much less than the distance of the baseplate to the liner. Therefore, the pool liner will not be contacted by the deformed baseplate. The lowering of the baseplate has been considered in the criticality evaluation and is specifically addressed in Chapter 4 of this report. Based on the impact event data in Table 7.4.1, the deep drop scenario 2 (through an internal cell over a support pedestal) is bounded by the postulated rack drop event since a dropped rack has more impact energy than a dropped fuel assembly.

7.5.3 Rack Drop Event

The maximum plastic strain of the SFP floor liner caused by the rack drop is calculated to be 0.0542, as shown in Figure 7.5.4, which is well below the failure strain of the liner (0.362) per Table 7.4.2, indicating that there is no rupture of the liner after the rack drop event. The SFP floor slab does, however, experience limited localized damage as shown in Figure 7.5.5 due to excessive compressive stress resulting from the impact load at the pedestal/liner interface. However, the localized damage does not represent any structural threat to the SFP slab. In addition, the dropped rack also experiences local plastic deformation in the cells adjacent to the pedestal as expected.

To obtain a quantitative assessment of the SFP slab global behavior under the rack drop condition, an additional rack drop analysis has been performed using LS-DYNA, which considers the entire SFP slab as well as a portion of the SFP walls directly connected with the slab as shown in Figure 7.5.6. The impact is conservatively assumed to occur at the center of the SFP floor irrespective of the actual layout of the racks in the SFP. Although the SFP is directly founded on grade, the vertical support offered by the underlying soil is not credited in the model for additional conservatism; the bottom of the SFP walls (flush with the SFP slab bottom surface) are vertically supported, making the SFP slab act as an elevated floor. The SFP concrete structure is modeled with solid elements, and the reinforcement of the slab is explicitly modeled as a thin shell at each face of the slab with an equivalent thickness. The SFP liner is also modeled using shell elements. Except for the rack drop location, the SFP is conservatively assumed to be occupied by fully loaded spent fuel racks. Prior to the rack drop event, the SFP floor is subjected to the dead load from the water and loaded spent fuel racks in the pool.

The global consequence of the rack drop accident is shown in Figures 7.5.7 through 7.5.9 and also summarized in Table 7.5.3.

Since the LS-DYNA simulation does not account directly for the thermal loading on the slab, the tensile stress in the bottom reinforcement due to the maximum thru-thickness temperature gradient is added to the calculated stress from LS-DYNA. Based on a maximum thru-thickness temperature gradient of 122°F, the induced bending moment in the 10-foot thick slab is 255,000 lbf-in/in, and the corresponding tensile stress in the bottom reinforcement is 7,280 psi. Adding this stress to the calculated value from LS-DYNA (9,379 psi), the total combined tensile stress in the bottom reinforcement due to the effects of dead load, thermal load, and the postulated rack drop is 16,659 psi, which is below the design basis yield strength of the steel reinforcement (40,000 psi). Therefore, the displacement of the SFP slab is less than its yield point displacement, and the ductility ratio of the SFP slab for this event is less than one. Since ductility ratios less than 1.3 are acceptable per Section 3.5.3 of the BVPS-2 UFSAR, it is concluded that the SFP slab has sufficient capacity to absorb the kinetic energy associated with the postulated rack drop. Thus, the postulated rack drop event does not undermine the global structural integrity of the SFP concrete slab.

The rack drop analyses described above also bound the effects of a rack drop in the cask pit area for the following reasons:

i) the impact velocity of the dropped rack is nearly equal to the terminal velocity of the rack in water so the difference in elevation between the SFP floor and the cask pit floor has no effect on the results;

ii) a direct impact between the dropped rack and the cask pit floor is not possible due to the presence of the cask pit rack platform which sits on the cask pit floor;

iii) a portion of the impact energy transmitted by the dropped rack will be absorbed by permanent deformation suffered by the cask pit rack platform (which will reduce the load transmitted to the cask pit floor);

iv) the cask pit rack platform transmits load to the cask pit floor through four (4) 32" × 22" support pads, which are significantly greater than the impact area considered in the SFP rack drop analyses (i.e., four (4) 4.5" diameter support pedestals);

v) although the cask pit floor is thinner than the SFP floor (7.5 ft vs. 10 ft), it has a much smaller span than the SFP floor (12 ft vs. 39.5 ft), and therefore the cask pit floor is stronger in bending.

The analyzed rack drop event in the SFP also bounds a free drop of the cask pit rack platform in the cask pit area based on the fact that the weight of the cask pit rack platform is less than the weight of the dropped rack by a factor of 6. The significant difference in weight compensates for the slightly increased drop height of the cask pit rack platform above the cask pit floor versus the drop height of the rack above the SFP floor (45.5 ft vs. 43 ft).

7.5.4 Uplift Force Evaluation

The uplift force evaluation shows that the rack is able to withstand the vertical uplift force of 5,000 pounds. Results of the analysis in [7.1.5] show that the maximum stress in the rack cell as a result of trying to pull the stuck fuel assembly out is only 6,500 psi which is well below the material yield strength. Therefore, the fuel racks are adequate to withstand a 5,000 lbf uplift load due to a stuck fuel assembly.

7.5.5 Fuel to Fuel Drop Event

The total number of fuel rods damaged from the impact on a stored fuel assembly in the rack by a dropped fuel assembly is calculated to be ten fuel rods for a drop height of 24" above the top of the rack. Figure 7.5.10 shows the deformed shape of the damaged fuel rods. The fuel damage in this Fuel-to-Fuel Drop Event is bounded by the existing Fuel Handling Accident Analysis provided for Beaver Valley Unit 2 License Amendment No. 121.

7.6 Conclusion

The drop accident events postulated for the Beaver Valley Power Station (BVPS) Unit No. 2 fuel pool were analyzed and found to produce localized damage well within the design limits for the racks. The shallow drop event is found to produce some localized plastic deformation in the top of the storage cell, but the region of permanent strain is limited to the portion of the rack structure situated above the top of the active fuel region. The analysis of the deep drop scenario 1 at cell locations selected to maximize baseplate deformation indicates that the downward displacement of the baseplate is limited to less than 2 inches, which ensures that a secondary impact of the fuel assembly with the pool liner would not occur. The rack drop analysis (which also bounds the deep drop scenario 2) shows that the concrete slab can maintain its structural integrity under the postulated impact of the heaviest rack in the pool. Only local concrete crushing is observed. The rack uplift force evaluation shows that configuration of the neutron absorber (Metamic) is not compromised from the configurations analyzed in the criticality evaluations discussed in Chapter 4. Additionally, it is demonstrated that the damage to the fuel assembly rods from the fuel-to-fuel impact drop is not severe.

It is therefore concluded that the proposed new Holtec high-density spent fuel racks for the BVPS Unit No. 2 fuel pool possess acceptable margins of safety under the postulated mechanical accidents.

7.7 References for Chapter 7

[7.1.1] "OT Position for Review and Acceptance of Spent Fuel Storage and Handling Applications," dated April 14, 1978, and addendum dated January 18, 1979.

[7.1.2] "Specification for Spent Fuel Storage Racks Replacement – Beaver Valley Unit 2", Design Specification No. 10080-DMS-0505, Rev. 1 (Holtec Report No. HI-2073792, Rev. 2).

[7.1.3] Not Used.

[7.1.4] "Summary and Evaluation of Low-Velocity Impact Tests of Solid Steel Billets onto Concrete Pads," Lawrence Livermore National Laboratory, UCRL-ID-129211, February 1998. Prepared for the NRC and also appears as NUREG /CR-6608.

[7.1.5] Holtec Report HI-2084123, "Structural/Seismic Analysis for Beaver Valley Unit 2", Rev. 5.

[7.1.6] Young, W.C., "Roark's Formulas for Stress & Strain", McGraw Hill Book Co., 6th Edition.

[7.1.7] Holtec Report No. HI-2084131, "Fuel Pool Structural Evaluation of Beaver Valley Unit 2", Revision 6.

[7.1.8] Holtec Report HI-90567, "Fuel Pool Structural Analysis of Beaver Valley Unit 1 with Maximum Density", Revision 2.

[7.4.1] Holtec Position Paper DS-307, "Construction of True Stress-True Strain Curves for LS-DYNA Simulations", Rev. 2 (previously submitted to the NRC under Docket 72-1032).

[7.4.2] NUREG-1864, "A Pilot Probabilistic Risk Assessment of a Dry Cask Storage System at a Nuclear Power Plant", March 2007.

[7.4.3] D.K. Morton, S.D. Snow, T.E. Rahl and R.K. Blandford, "Impact Testing of Stainless Steel Material at Room and Elevated Temperatures," ASME Pressure Vessel and Piping Conference, San Antonio, TX, PVP2007-26182, ASME, NY, NY, July 2007.

Table 7.4.1

IMPACT EVENT DATA

Case	Impactor Weight (lb)	Impactor Type	Drop Height (in)	Impact Velocity (in/sec)
1. Shallow drop event	2,450	Fuel assembly	24 inches above the top of rack	129.2
2. Deep drop event scenario 1 (away from pedestal)	2,450	Fuel assembly	„	275.6
3. Deep drop event scenario 2 (above pedestal)	2,450	Fuel assembly	„	105.8
4. Rack drop event	24,700	Rack	From top of water level in the pool	222.0
5. Gate drop event	4,020	Gate	24 inches above the top of rack	119.1
6. Fuel assembly on Fuel assembly drop scenario (above rack)	2,450	Fuel Assembly	24 inches above the top of rack	129.2

Table 7.4.2

MATERIAL DEFINITION

Material Name	Material Type	Density (pcf)	Elastic Modulus (psi)	Stress		Strain	
				First Yield (psi)	Failure (psi)	Elastic	Failure
Stainless Steel Rack Walls, Rack Female Pedestal and Spent Fuel Pool Liner	SA240-304L	490	2.799e+07	2.270e+04	6.805e+04	8.110e-04	3.620e-01
Zircaloy Fuel Cladding	--	404	1.040e+07	8.05e+04	9.20e+04	7.740e-03	2.000e-02
Stainless Steel Male Pedestal	SA564-630	490	2.823e+07	1.092e+05	1.400e+05	3.868e-02	1.400e-01
Concrete†	f'_c=3,000 psi	150	3.122e+06	--	--	--	--

Notes:

1. Material strength values for SA240-304L and SA564-630 are evaluated at 150°F, which corresponds to the SFP bulk water temperature during a normal full core offload with both Fuel Storage Pool cooling system pumps and heat exchangers operating.
2. Properties at 200^{0}F were conservatively used for the deep drop scenario 1 analysis.

† The concrete is modeled as recommended in NUREG /CR-6608 [7.1.4].

Table 7.4.3

VALUES OF "K" AND "n"

Material Type	Reference Temperature (°F)	K (psi)	n
Base Metal (SA-240 304L)	150	1.21×10^5	0.235
Weld Metal (Type 308)	150	1.21×10^5	0.235

Table 7.5.1

RESULTS FOR SHALLOW FUEL ASSEMBLY DROP ONTO PERIMETER CELL

Impact Duration (sec)	0.0375
Peak Impact Force (lbf)	83,361
Fuel Assembly Vertical Displacement (in)	1.2
Plastic Deformation Measured from the Rack Top (in)	12.0

Table 7.5.2

RESULTS FOR SHALLOW FUEL ASSEMBLY DROP ONTO INTERIOR CELL

Impact Duration (sec)	0.095
Peak Impact Force (lbf)	32,915
Fuel Assembly Vertical Displacement (in)	3.15
Plastic Deformation Measured from the Rack Top (in)	10.0

Table 7.5.3

RESULTS OF GLOBAL RACK DROP ANALYSIS

Maximum (local) plastic strain of the SFP floor liner	0.0163
Maximum stress of the SFP concrete slab bottom reinforcement	9,379 psi
Maximum compressive stress of the SFP concrete slab	6,803 psi

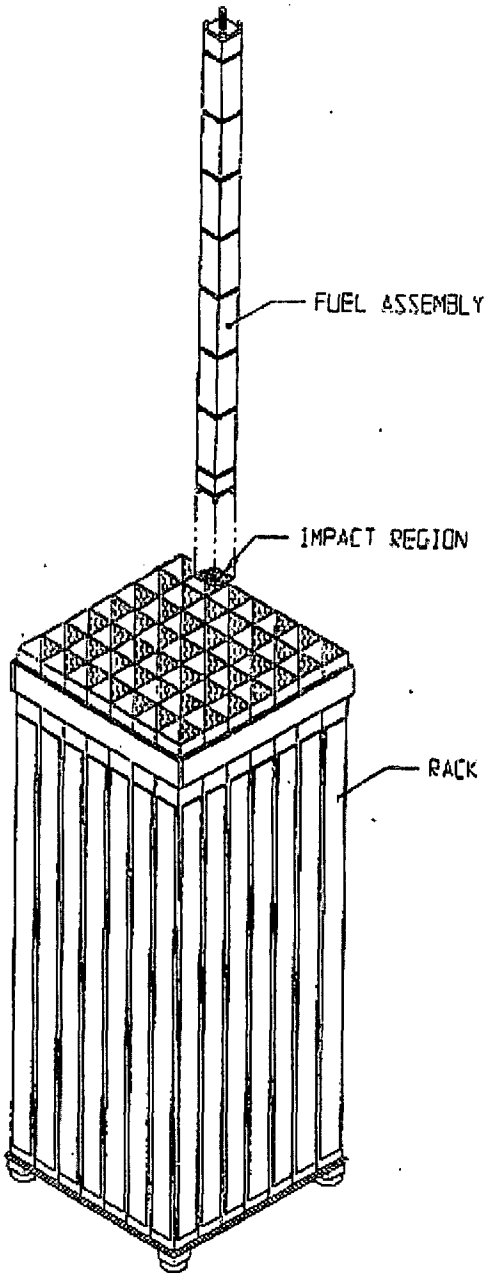

Fig. 7.2.1 Schematics of the Straight Shallow Drop on a Rack Cell

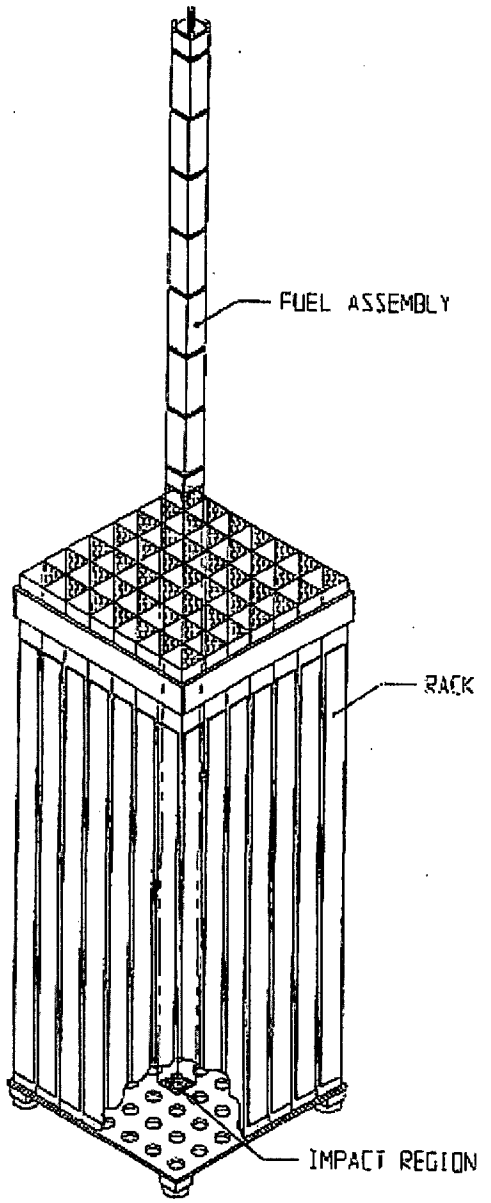

Fig. 7.2.2 Schematics of the "Deep" Drop (Scenario 1) on a Center Cell Location

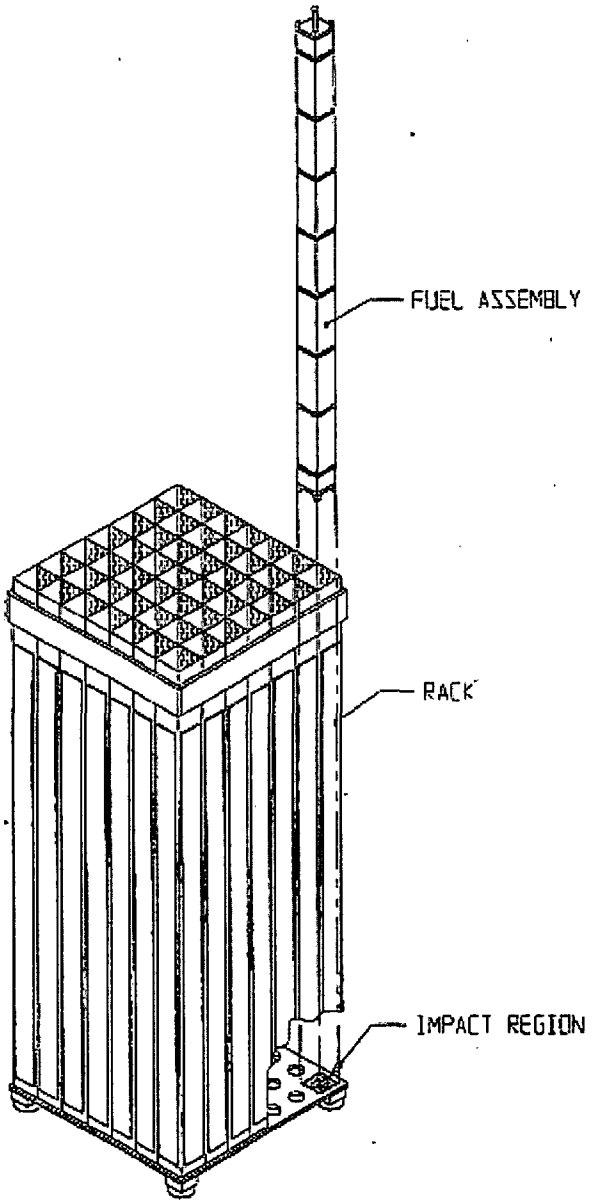

Fig. 7.2.3 Schematics of the "Deep" Drop (Scenario 2) on a Support Leg Location

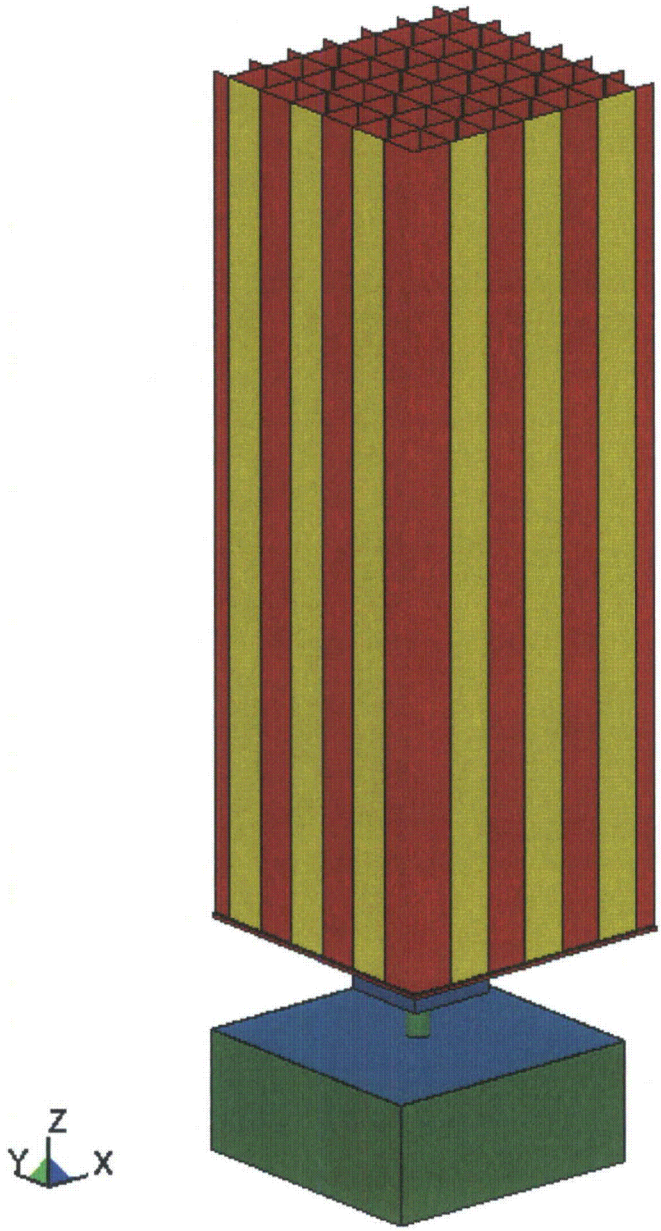

FIGURE 7.2.4: Schematic of Rack Drop Scenario

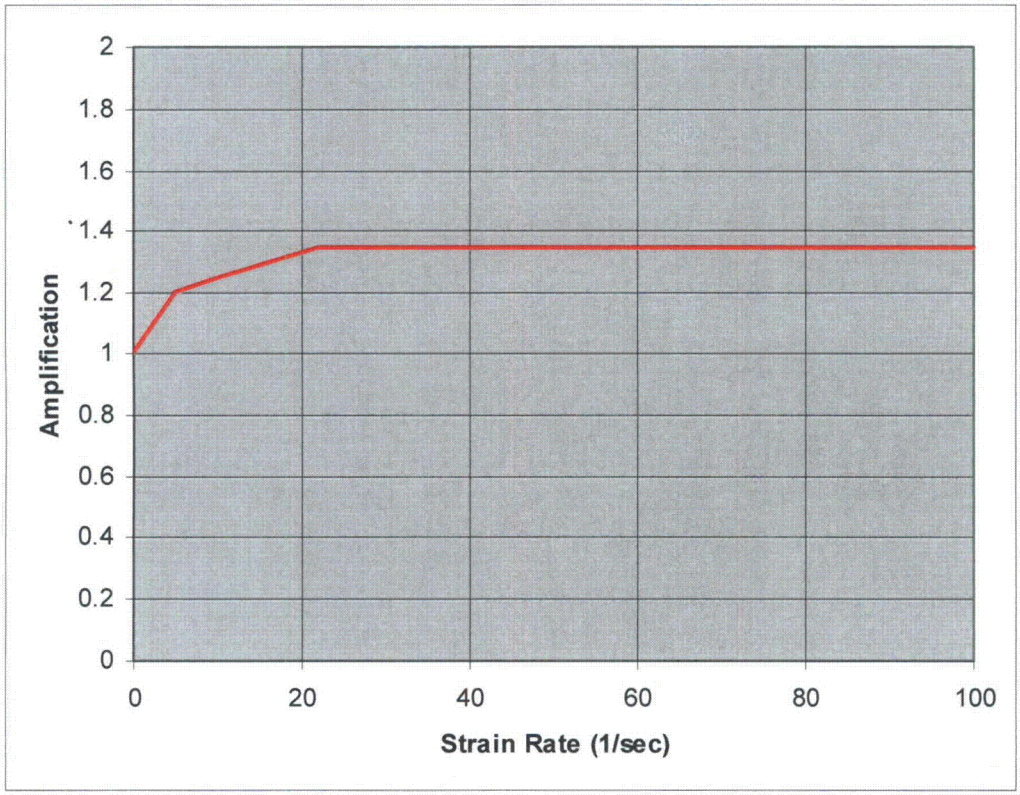

Figure 7.4.1: Strain Rate Amplification Curve for Base Metal Material

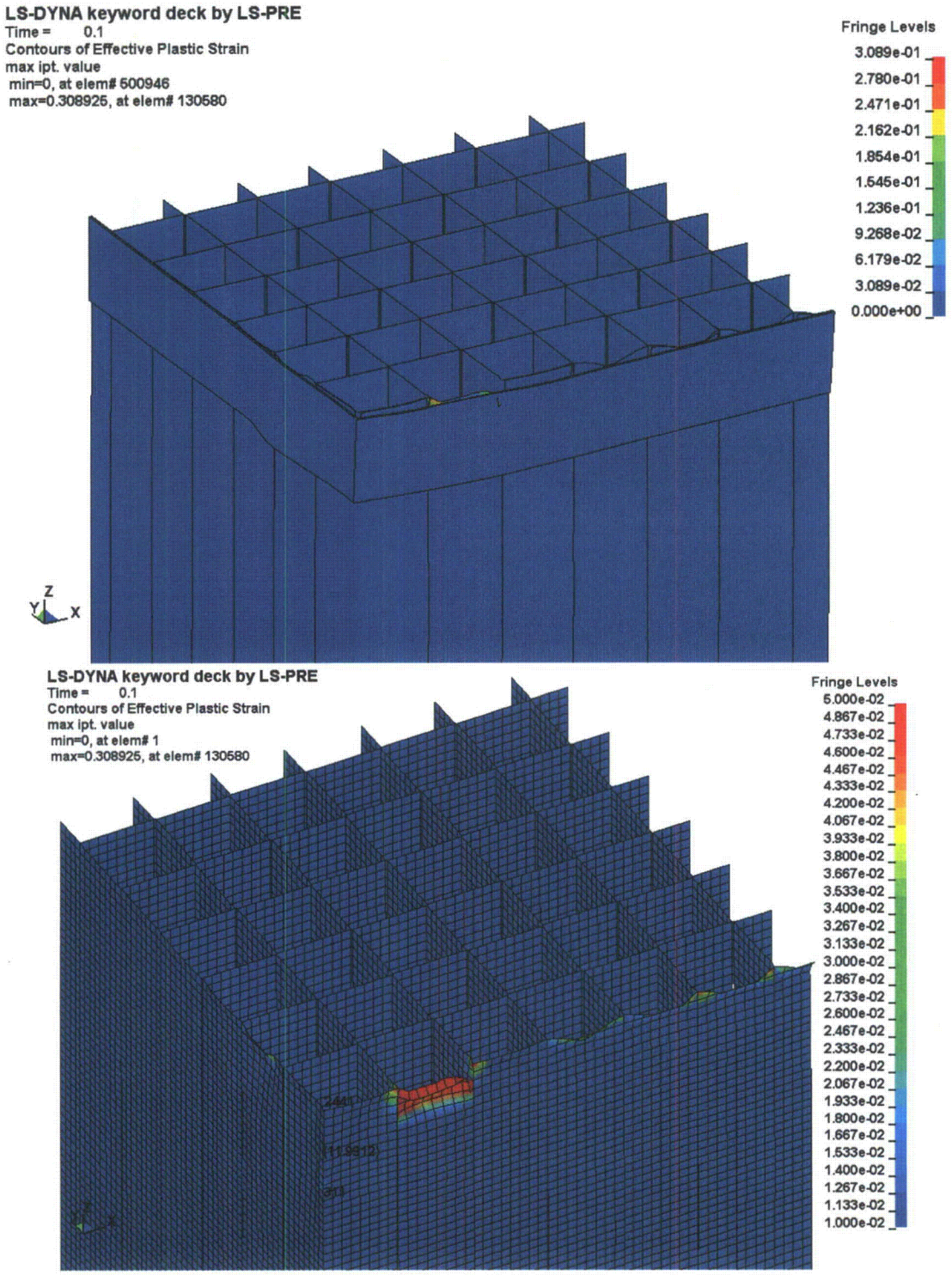

Figure 7.5.1: Deformed Shape of Spent Fuel Rack Due to Perimeter Cell Impact

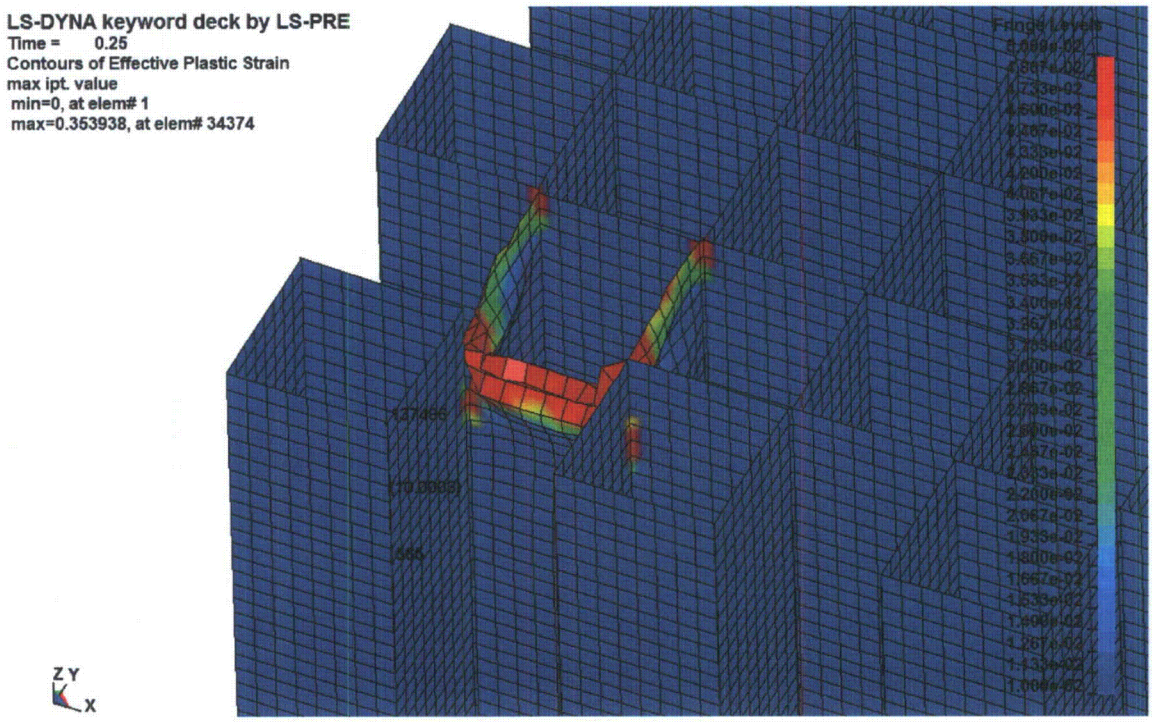

Figure 7.5.2: Deformed Shape of Spent Fuel Rack Due to Interior Cell Impact

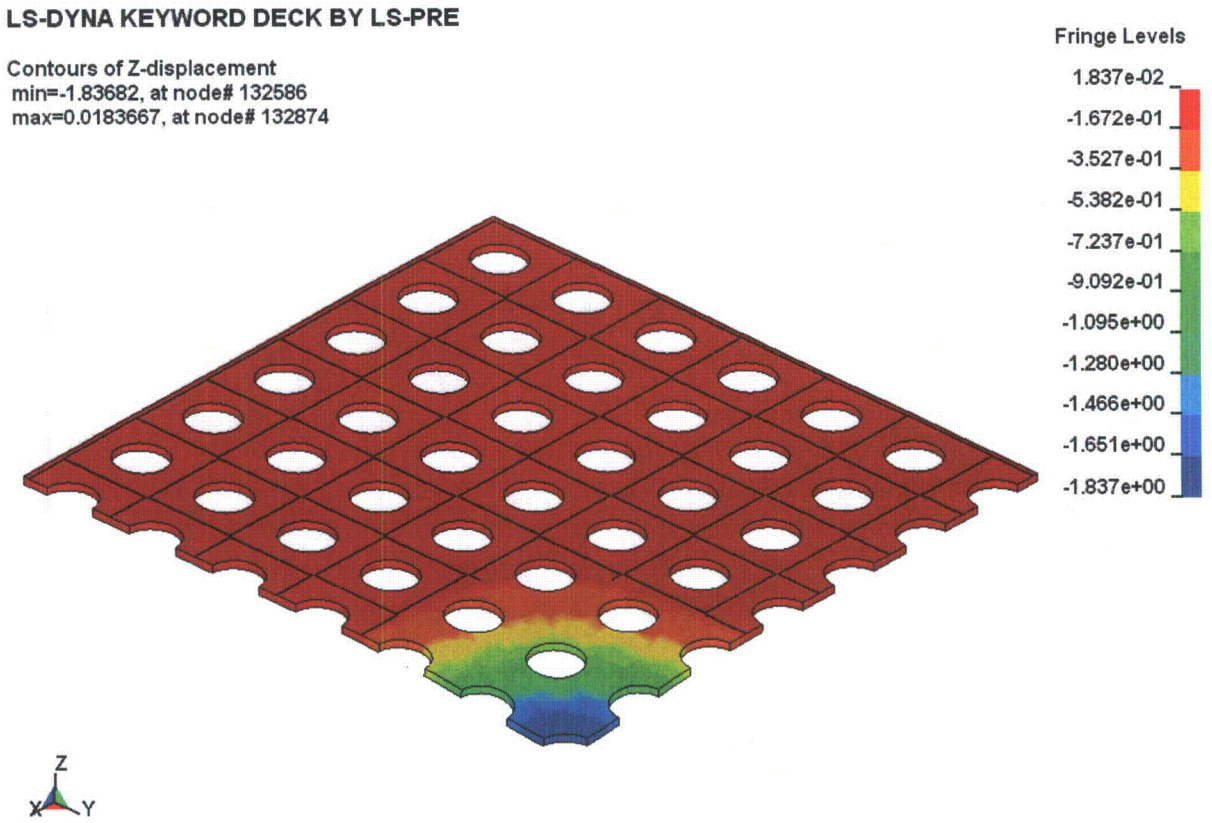

Figure 7.5.3: Peak Baseplate Vertical Deflection – Deep Drop Scenario 1

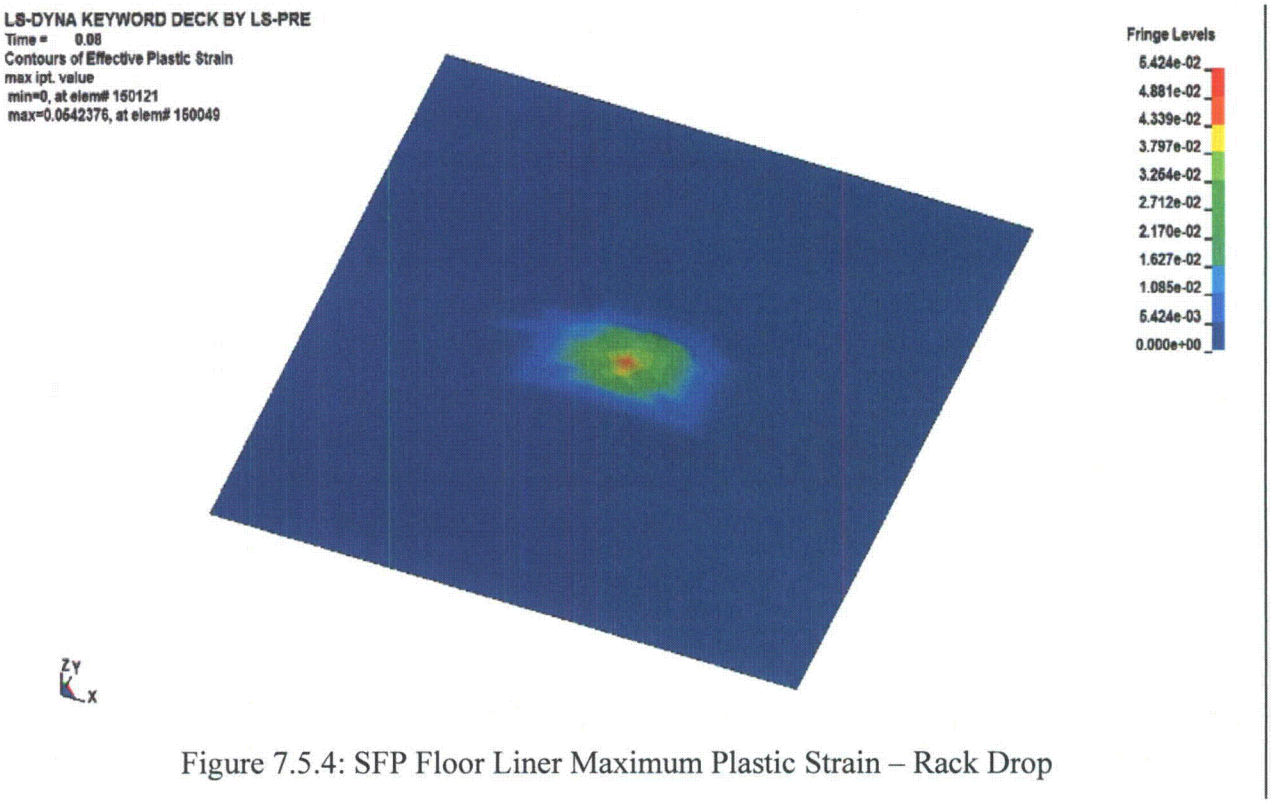

Figure 7.5.4: SFP Floor Liner Maximum Plastic Strain – Rack Drop

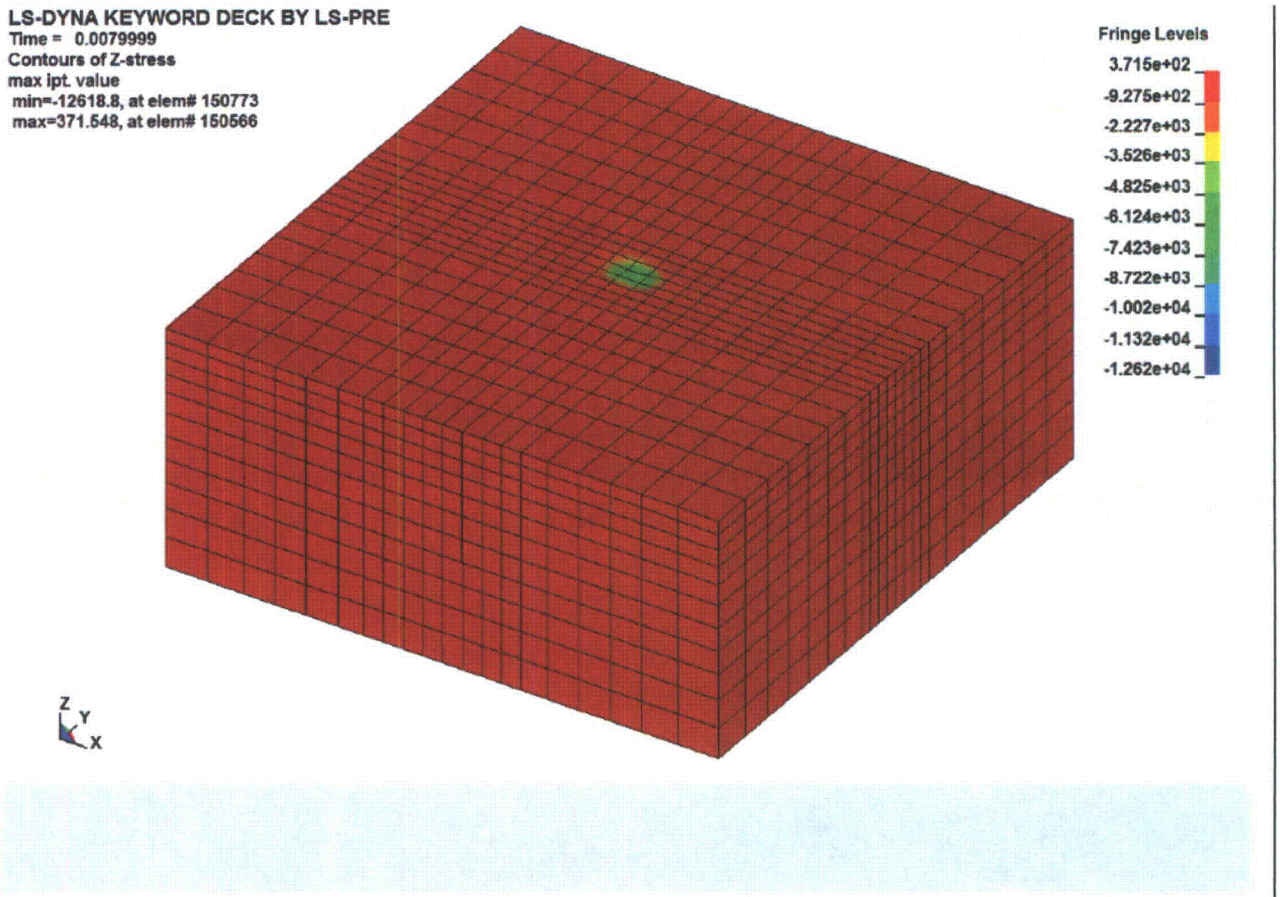

Figure 7.5.5: SFP Floor Concrete Slab Maximum Compressive Stress – Rack Drop

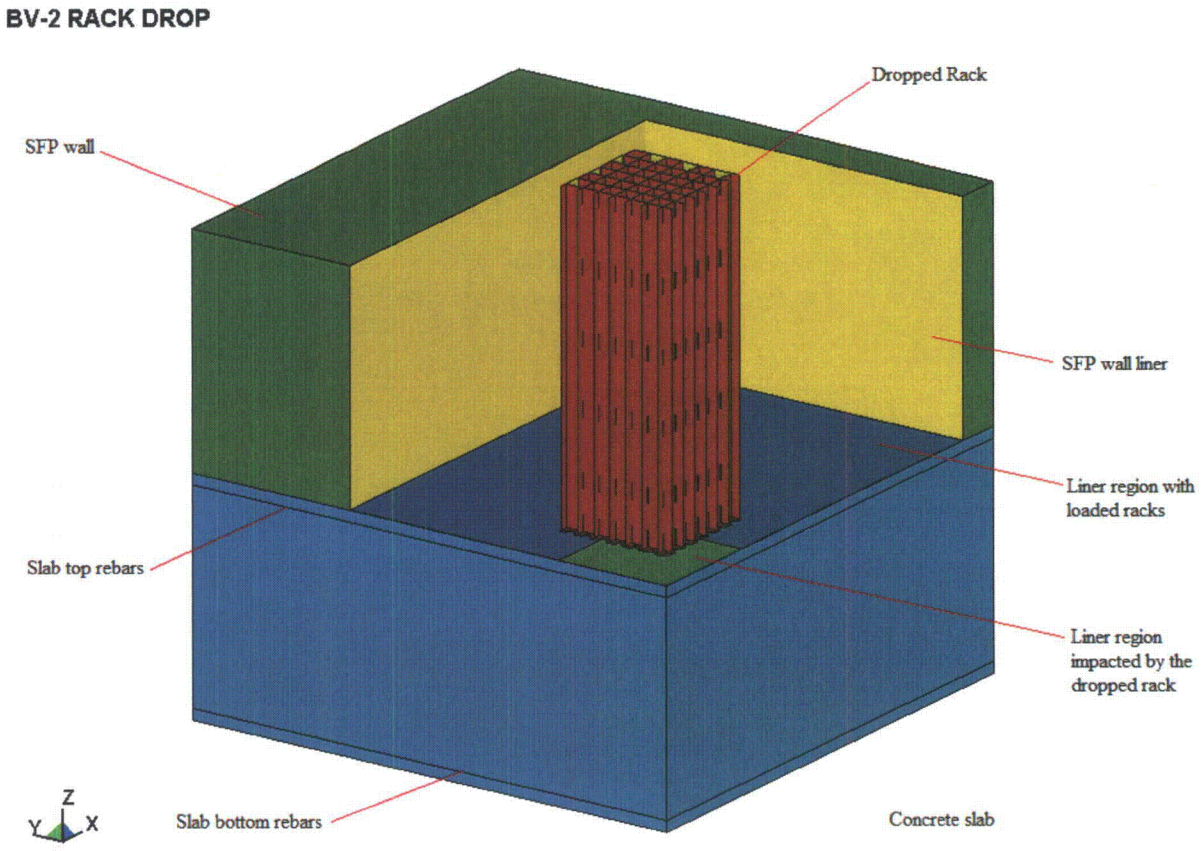

Figure 7.5.6: Rack Drop LS-DYNA Model

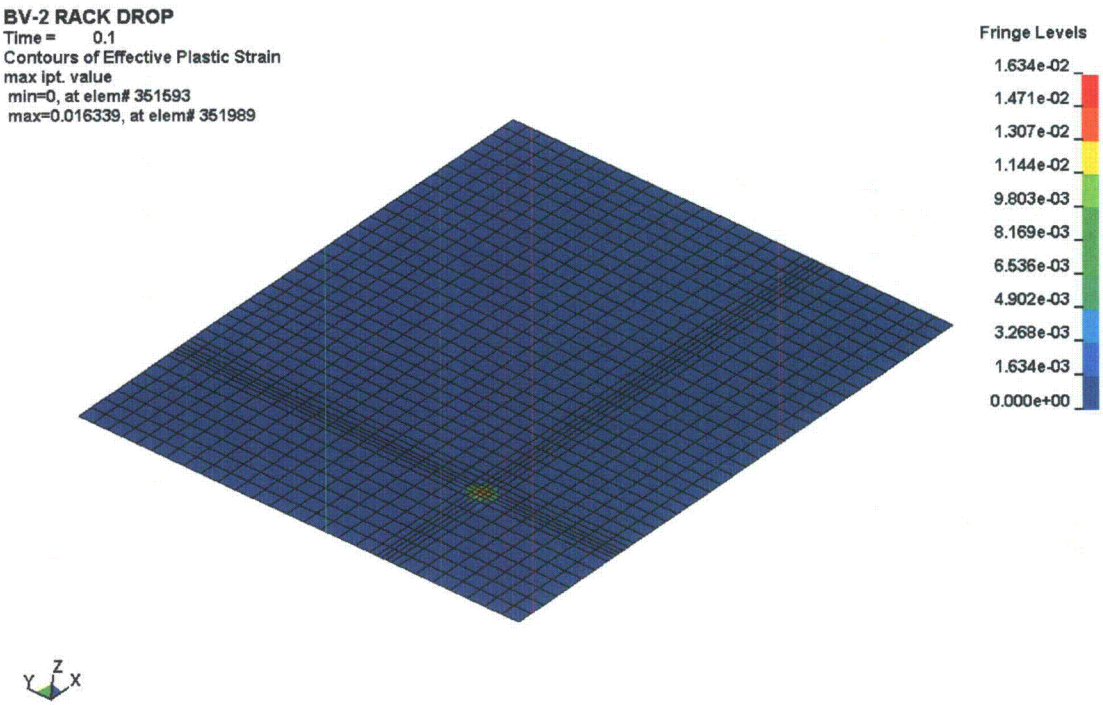

Figure 7.5.7: Maximum Plastic Strain of the SFP Floor Liner after the Rack Drop Accident

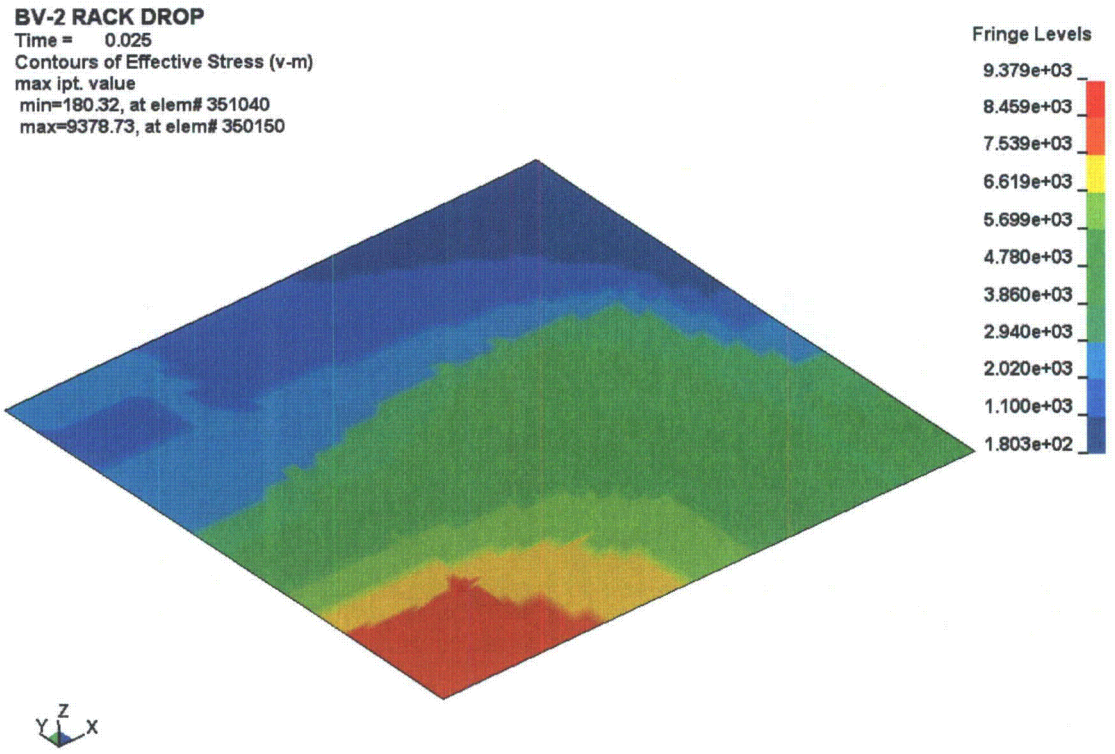

Figure 7.5.8: Maximum Stress in the Bottom Reinforcement Due to the Rack Drop Accident

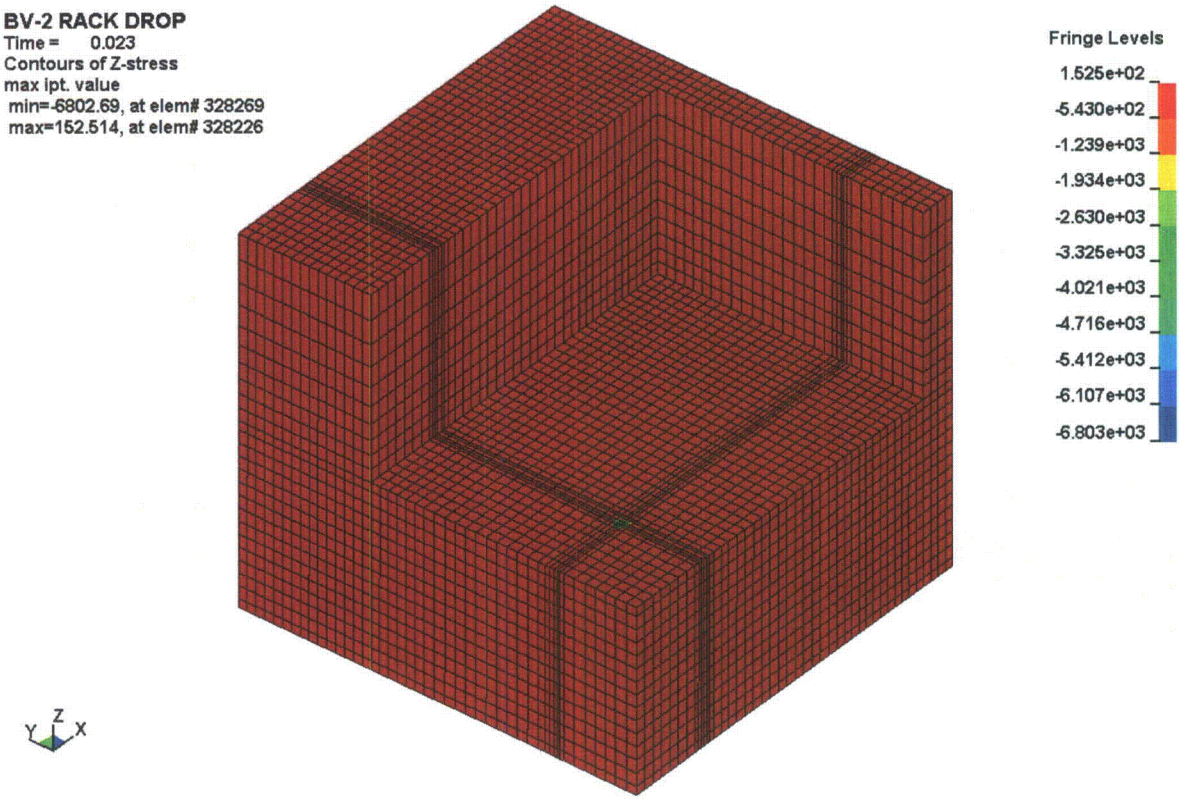

Figure 7.5.9: Maximum Compressive Stress of the SFP Concrete Slab Resulting Due to the Rack Drop Accident

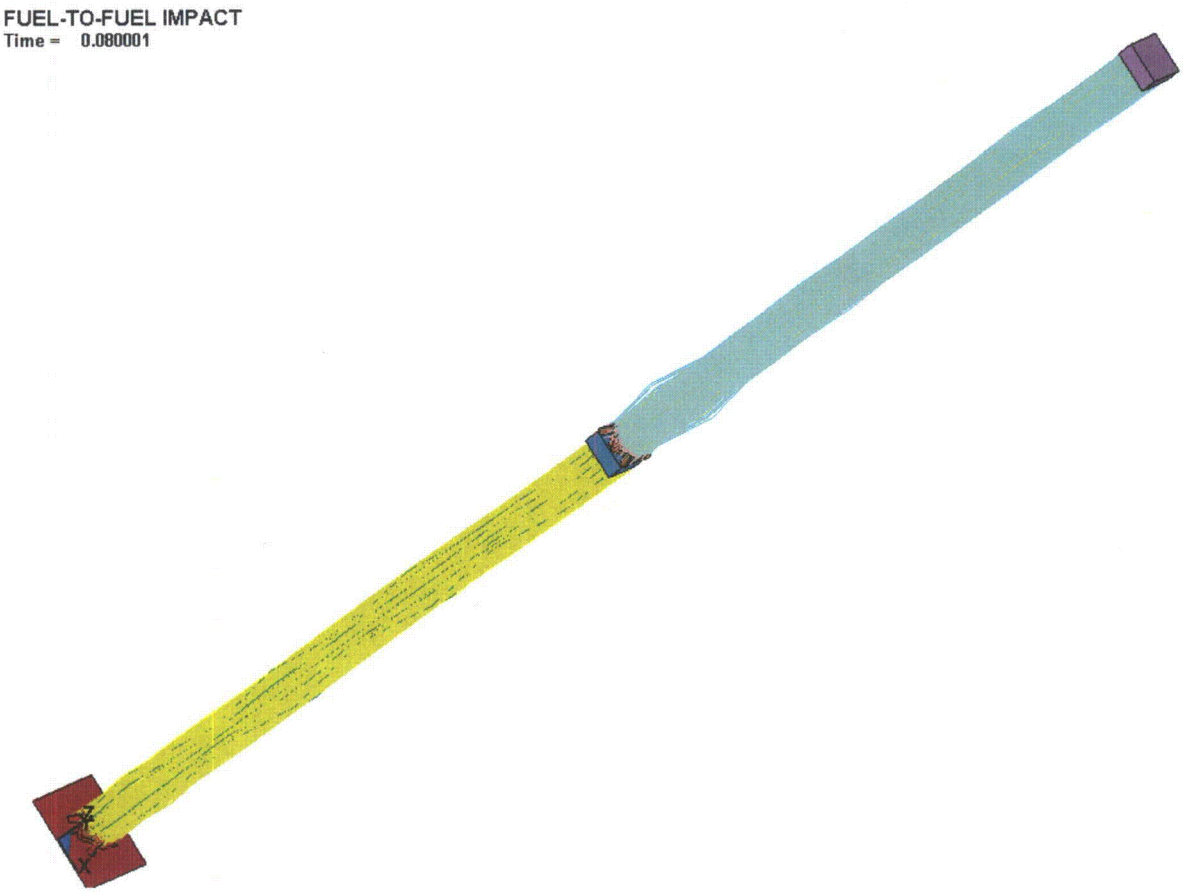

Figure 7.5.10: Deformed Shape of Fuel Rods (rack cell not shown) – Fuel-to-Fuel Impact